Dynamics of Vortex evolution in a 2D baffled tank

Wu, Chih-Hua[a], Faltinsen, Odd Magnus[b], and Chen, Bang-Fuh[c,*]

[a] Formerly, Asia-Pacific Ocean Research Center (APORC), National Sun Yat-sen University, Taiwan; now Institute of High Performance Computing, A*STAR, 1 Fusionopolis Way, #16-16 Connexis north,138632, Singapore

[b] Department of Marine Technology, NTNU, Trondheim, Norway

[c*] Asia-Pacific Ocean Research Center (APORC), National Sun Yat-sen University, Taiwan

*chenbf@mail.nsysu.edu.tw ; corresponding author

Tel.: +886 7 5252000x5065; fax: +886 7 5255065

Abstract

A finite difference method with coordinate transformation and fictitious cell approach were used to analyze the vortex generation and shedding phenomenon for sloshing liquid in 2D tanks with baffles. The detailed description of the dynamics of vortex evolution for sloshing fluid in a tank with baffles is seldom seen in the literatures and is firstly reported in this study. The exploration of liquid sloshing in a 2D tank with vertically bottom-mounted baffles is demonstrated. The benchmark tests of a tuned liquid damper (TLD) solved by the present numerical scheme show good agreements with the reported results. The experimental measurement is also carried out in this study and the present numerical simulation has excellent accuracy according to the comparison between the computational results and experimental measurement. The evolution of vortices inside a baffled tank in terms of vortex generation, vortex shedding and the trajectories of vortices are analyzed. Four phases of interaction processes of vortices are categorized in this work. The comprehensive discussions include the evolution of vortices and vortex shedding around the baffle tip, the vortex size generated in the vicinity of the baffle tip, the shedding frequency of the vortices, and the interaction of vortices inside the tank with various heights of the baffles and liquid depths. The vortex shedding phenomenon in the vicinity of the baffle tip is tightly correlated with the strength of the vertical jet along the baffle walls and the excitation frequency of the tank. Vortex size is closely correlated with the baffle height. When the baffle height is small ($d_b \leq 0.2\ d_0$), the vortex size mainly grows in the horizontal direction. Instead, the vortex size dominantly develops in the vertical direction as $d_b \geq 0.3\ d_0$. The period of the generation and shedding of vortices near the baffle tip is nearly about one half of the excitation period of the tank. The dynamics of vortex evolution is closely related to the growth and the hydrodynamic interaction of the vortices and sensitively depends on the baffle height, liquid depth, excitation frequency, and excitation displacement of the tank.

Keywords: baffled tank, sloshing flow, vortex evolution, vortex shedding

1. Introduction

Sloshing must be considered for most of moving vehicles and structures containing a liquid with a free surface, such as tankers on highways, liquid oscillations in large storage tanks caused by earthquakes, sloshing of liquid cargo in ocean-going vessels, and the motion of liquid fuel in aircraft and spacecraft etc. The large amplitude movement of the liquid can create high impact pressures on the tank walls, which in turn might cause structural damage and may even create moments that affect the stability of the vehicles. Sloshing effects are also needed to be considered in the design loads for LNG (liquefied natural gas) storage tanks. Sloshing in a container can be used to dampen out wind-induced motions of tall buildings. A tuned liquid damper, TLD, is a well-known concept in the civil engineering world and is used to suppress horizontal vibrations of structures. That is, the liquid tank can be used as a damper that the proper tuned liquid tank may mitigate earthquake and wind induced vibration of tall building or long span bridge. Therefore, a liquid tank is also frequently used as a TLD to reduce possible violent oscillation of the structures (Banerji *et* al. [1][2], Sun *et* al. [3], Reed *et* al. [4], Fujino *et* al. [5], and Marivani and Hamed [6]). The simple idea is the sloshing frequency of the liquid in a tank can be tuned to give a desired reaction to reduce the vibration of the structures attached with liquid tanks.

Numerous analytical, numerical and experimental analyses of the seismic response of fluid sloshing in a baffled tank have been published. Koh et al. [7] studied the effects of rectangular liquid dampers on the reduction of structural vibration during earthquakes but the free surface condition and the base shear were approximated empirically. Kim [8] and Kim et al. [9] solved the primitive Navier-Stokes equations by a SOLA scheme and studied the sloshing flow in tanks with and without internal baffles. Both reports ignored surface tension and the tangential stresses at the free surface, and assumed a zero hydrodynamic pressure at the free surface. Warnitchai and Pinkeaw [10] reported a mathematical model compared with experimental investigations for a rectangular tank with flow-damping devices. The vertical flat plate and wire mesh screen can cause significant damping effects on sloshing waves. Isaacson and Premasiri [11] developed the mathematic solutions and made experiment investigations to describe the hydrodynamic damping due to baffles in a fluid-filled rectangular tank undergoing horizontal motions. The average rate of energy dissipation due to flow separation around baffles and the total energy of sloshing waves were used to estimate the hydrodynamic damping. More recently, Faltinsen and Timokha [12] estimated in detail the damping effect of sloshing fluid due to internal structures (baffles, screens, plate, poles) by an analytic formula.

For numerical studies associated with TLD, the finite element method (FEM) is a popular numerical method in solving the baffled tank. Cho and Lee [13,14], studied the sloshing liquid in a baffled tank by a nonlinear finite element method. Biswal *et al.* [15] applied FEM on computing the non-linear sloshing response of liquid in a two-dimensional rectangular tank and circular cylindrical container with rigid baffles. The effect of baffle parameters including length, numbers and position on sloshing response were discussed. Liu and Lin [16] used NEWTANK to investigate liquid sloshing in baffled tank with Large-eddy-simulation (LES). In their study, the vertical baffle is a more effective tool in reducing the sloshing amplitude. In the same year, A BEM (Boundary element method) model for liquid sloshing in a baffled tank was adopted by Firouz-Abadi *et al.* [17]. The determinations of the natural frequencies and mode shapes of liquid sloshing in baffled tanks with arbitrary geometries were investigated. However, the potential flow assumption used in BEM cannot predict the effect of energy dissipation due to viscous sloshing and flow separation. Panigrahy *et al.* [18] did a series of experiment in a developed liquid sloshing with and without different types of baffles under various filled depth. The pressure developed on the tank walls and the free surface displacement of water from the mean static level were measured and analyzed. They concluded that the introduction of baffles in the tank decreases effectively the sloshing displacement because the sharp-edged baffles could dissipate the kinetic energy by generating turbulence in the flow and the type of ring baffles are the most effective device to reduce sloshing energy.

Generally speaking, vortices are developed near the tip of baffles. Lin *et al.* [19] reported the experimental study related to a solitary wave propagating over a submerged vertical plate and the evolution of vortices were categorized into four interaction process: formation of a separated shear layer, generation and shedding of vortices, formation of a vertical jet, and the impingement of the jet onto the free surface. Accordingly, the correlation between the movement of baffles and flow field due to liquid sloshing might be the clue to investigate the evolution of vortices around the baffle tip.

A 2D tank with internal baffles is considered in this work .The treatment of flow field around baffles is carried out by the combination of a fictitious cell approach, which is similar to the ghost cell approach [20], and the time-independent finite difference method [21]. Section 2 introduces the equations of motion which are written in a moving frame of reference attached to the accelerating tank. The fully non-linear free surface boundary conditions are listed in this section. Besides, the fictitious cell approach is implemented to deal with the interfaces of fluid and structure (baffle, tank bottom and tank walls). The comprehensive benchmark tests of the present numerical scheme are demonstrated in section 3. The investigations of 2D tanks with baffles are also dissected in the section. Section 4 summarizes the key conclusions.

2. Mathematical formulation and numerical approach

In this work, a rigid tank with partially filled fluid is considered and analyzed by a time-independent finite difference method [21] to simulate the movement of sloshing liquid with baffles. As illustrated in Fig. 1, the breadth of the tank is L, *h(x,t)* is the elevation of free surface measured from tank bottom and d_0 and d_b are the still water depth and the baffle height, respectively. The Navier-Stokes equations are written in a moving coordinate system and can be expressed as

$$\frac{\partial u}{\partial t}+u\frac{\partial u}{\partial x}+v\frac{\partial u}{\partial y}=-\frac{1}{\rho}\frac{\partial p}{\partial x}-\ddot{x}_C+\upsilon(\frac{\partial^2 u}{\partial x^2}+\frac{\partial^2 u}{\partial y^2}) \tag{2.1}$$

$$\frac{\partial v}{\partial t}+u\frac{\partial v}{\partial x}+v\frac{\partial v}{\partial y}=-g-\frac{1}{\rho}\frac{\partial p}{\partial y}-\ddot{y}_C+\upsilon(\frac{\partial^2 v}{\partial x^2}+\frac{\partial^2 v}{\partial y^2}) \tag{2.2}$$

where *u,* and *v* are the relative velocity components in *x* and *y* directions, $\ddot{x}_C$, and $\ddot{y}_C$ are the acceleration components of the tank in *x,* and *y* directions; *p* is the pressure, ρ is the liquid density, υ is the kinematic viscosity of the fluid and g is the acceleration due to gravity.

The continuity equation for incompressible flow is

$$\frac{\partial u}{\partial x}+\frac{\partial v}{\partial y}=0 \tag{2.3}$$

The kinematic condition states the fluid particles at free surface remain on the free surface and is expressed as

$$\frac{\partial \eta}{\partial t}+u\frac{\partial \eta}{\partial x}=v \tag{2.4}$$

where $\eta = h(x,t)-d_0$ is the elevation of free surface measured from the initial water depth. The dynamic condition requires that the normal stress is equal to the atmospheric pressure and the two tangential stresses are zero along the free surface boundary. The dynamic conditions can, then, be derived and expressed as follows [16]:

$$P_F = \frac{y}{Fr^2}+\frac{2[u_x\eta_x^2+v_y-(u_y+v_x)\eta_x]}{\mathrm{Re}(\eta_x^2+1)} \tag{2.5}$$

$$u_y = -v_x + \frac{2(u_x-v_y)\eta_x}{1-\eta_x^2} \tag{2.6}$$

where F_r and Re are the Froude number and the Reynolds number, respectively, and are defined as

$$F_r = \frac{u_m}{\sqrt{gd_0}}$$
$$\mathrm{Re} = \frac{u_m d_0}{\upsilon} \tag{2-7}$$

where $u_m = \omega x_0$ (ω is the angular velocity and x_0 is the excitation displacement of the tank) is the maximum velocity of the tank. The subscript x or y means a partial derivative along the x or y directions for all the quantities. In the present study, Eq. (2.5) is used to determine the hydrodynamic pressure at the free surface, while Eq (2.6) is used to calculate velocity u at the free surface.

Taking partial derivatives of equations (2.1) and (2.2) with respect to x and y respectively, and summing the results, one can obtain the following equation to solve for the pressure.

$$\frac{\partial^2 p}{\partial x^2}+\frac{\partial^2 p}{\partial y^2}=-\rho\frac{\partial}{\partial x}\left(u\frac{\partial u}{\partial x}+v\frac{\partial u}{\partial y}\right)-\rho\frac{\partial}{\partial y}\left(u\frac{\partial v}{\partial x}+v\frac{\partial v}{\partial y}\right) \tag{2.8}$$

In the present study, we used simple mapping functions to remove the time-dependence of the free surface in the fluid domain. The time-varying fluid surface, tank walls and tank bottom can be mapped onto a square by the proper coordinate transformations. The convenience of coordinate transformation is to map a wavy and time-dependent fluid domain onto a time-independent unit square domain. As listed in Fig. 1, the distance from the tank west wall to the baffle center is X_b and the distance between the free surface and the baffle tip is Y_b. We divide the fluid domain into four parts based on the location and the height of the baffle. The mapping functions of coordinate transformation of four parts can be expressed as

$$x_1^*=\frac{x_1}{X_b},\qquad x_2^*=\frac{x_2}{L-X_b},\qquad y_1^*=1-\frac{y_1+d_0-Y_b}{h(x,t)-Y_b},\qquad y_2^*=-\frac{y_2}{Y_b} \tag{2.9}$$

Through the above mapping functions, one can make the west wall to $x_1^*=0$ and the baffle center to $x_1^*=1$ and $x_2^*=0$ and the east wall to $x_2^*=1$; the free surface to $y_1^*=0$ and the baffle tip to $y_1^*=1$ and $y_2^*=0$ and the tank bottom to $y_2^*=1$. The advantage of the transformations is to avoid the internal structures surrounded by the irregular meshes. Further, combining with the stretching transformation [23], the stretching grids can be arranged around the structure boundaries with the sharp corners. The thickness of baffle is negligibly small compared with the length of the tank and the baffle width only occupies about the size of two meshes in this study. Furthermore, the fictitious cell approach [24] combined with the present numerical scheme is demonstrated in order to deal with the fluid-structure domain for a tank with internal structures.

Central difference approximations are used for the space derivatives, except at the boundary where forward or backward differences are employed. A staggered grid system is used in the analysis.

The Crank-Nicholson second order finite difference scheme and the Gauss-Seidel point successive over-relaxation iterative procedure are used to calculate the velocity and pressure, respectively. The iterative procedure is associated with the accuracy of the numerical results and the convergence speed of the present numerical scheme. In order to reduce the iterative numbers of each time step, a developed new iterative procedure similar to SIMPLEC algorithm is used [25] and a special treatment of iterative procedure on the implicit part of Crank-Nicholson scheme was implemented. The convergence checks for pressure and velocity are made together at every iteration to couple the fluid pressure and velocity in the simulation. In this way, the iteration numbers decreases and the convergence speed significantly increases by comparing to [21]. The convergence criterion for the iteration of u, v, and p is 10^{-5}, while for η it is set to 10^{-7}.

The accuracy of the numerical results significantly depends on the spatial grid resolution and the selected time step. The numerical errors can be reduced if the time step is restricted by the condition given in equation (2.10)

$$\begin{aligned} &\Delta t < \min\left\{\frac{\Delta x_{\min}}{|u_{i,j}|}, \frac{\Delta y_{\min}}{|v_{i,j}|}\right\} \\ &v\Delta t < \frac{1}{2}\frac{\Delta x^2{}_{\min}\Delta y^2{}_{\min}}{\Delta x^2{}_{\min} + \Delta y^2{}_{\min}} \end{aligned} \tag{2.10}$$

Equation (2.10) implies that a fluid particle cannot move more than one cell in a single time step. The second ensures that the diffusion of momentum is not significant over more than one cell in one time step.

3. Results and discussions

The validation and verification of the developed numerical scheme are made in section 3.1 before a large quantity of numerical simulations is planned. In order to validate the present numerical results, a serious of benchmark tests are rigorously compared with the reported experimental, analytical and numerical results for a tank with a vertically tank bottom-mounted baffles. Moreover, the convergence (stability) study is carried out to verify the quality of the numerical results obtained in the study. The comprehensive investigations of vortex evolution, vortex size, and vortex shedding around the baffle tip are demonstrated in sections 3.2 and 3.3.

3.1 Benchmark tests

3.1.1 The convergence study

The convergence study for a vertically tank bottom-mounted baffle in a 2D tank with sloshing are presented in this section. The ratio of baffle height and still water depth is defined as $\xi = d_b / d_0$. Figs. 2 (a) and (b) present the influence of grid numbers with various time steps (d*t*) during the transient and steady-state periods, respectively and only minor difference is found for different combinations of grid numbers and time steps. Based on the results of convergence study, the mesh number (X x Y) = 200 x 80 and time step d*t* = 0.001 s are applied in the following simulations.

3.1.2 The experimental measurement and comparison

The experimental study related to liquid sloshing in baffled tanks is also carried out in this work. As illustrated in Fig. 3(a), the photograph of the baffled tank attached to a shaking table can be moved back and forth with various excitation angles by an AC motor. The excitation direction of shaking table is designed to be altered by an aluminum alloy rotational table. The maximum moving distance (*r*) of the shaking table is $\pm$30mm and the highest revolutions of the motor is 2000 r.p.m .The frequency level depends on the limitation of the maximum velocity implemented by the AC motor and the motor reducer. In this experimental work, the maximum velocity ($V_m = \omega r$) of the shaking table is about 30 mm/s that indicates if the excitation displacement (*r*) becomes large, the corresponding excitation frequency has to be reduced. The material of the baffled tank is acryl with 20mm thickness and that of the baffle is fibreglass that can avoid the occurrence of baffle deformation due to hydrodynamic forces. The definition sketch of the baffled tank is illustrated in Fig. 3(b) and the positions of wave probes (P_1, P_2) are presented as well. Only surge motion is implemented to compare with the present numerical simulation of 2D baffled tank. The comparison between the experimental measurement and the numerical result for the baffled tank with d_b/d_0=0.5, d_0/L=0.5, forcing frequency ω_x=1.0ω_1 (ω_1 is the first natural mode of the partially filled tank) and excitation displacement of 0.004L are depicted in Fig. 4 and the agreement is excellent.

The influence of the single baffle inside a tank on the natural frequency of the container is described by an asymptotic formula based on potential flow of an incompressible liquid [12] which assumes d_b/L<<1 and $d_b/\, d_0$<<1 and it can be expressed as

$$\frac{\tilde{\omega}_m^2}{\omega_m^2} = 1 - \frac{2\pi \sin(\pi m(x_0 + \frac{1}{2}L)/L}{\sinh(2\pi m d_0 / L)} (\frac{d_b}{L})^2 \tag{3.1}$$

where m is the mode of natural frequency. $\tilde{\omega}_m$ and ω_m are the natural mode of the liquid tank with and without baffles, respectively.

Based on Welch's method [26], the power spectral density (PSD) analysis on free surface elevation is implemented here to obtain the frequency of maximum response or the lowest natural frequency (ω_{b1}) of the baffled tank. Fig. 5 compares the present numerical results, experimental measurements, BEM results, and those predicted by the formula [12] for the lowest natural frequency of the baffled tank and the agreement is good when $\xi = d_b/\, d_0 \leq 0.3$. For larger ratio of ξ , the asymptotic formula is inadequate to predict the influence of internal baffles on the natural frequency of the tank. The numerical results reported by Firoua-Abadi *et al*. [17] are based on a potential flow theory. The viscous effect and the energy dissipation are, therefore, unable to be explored by the method. As ξ is close to 1, which means the baffle is beneath the mean free surface for a small distance, the obvious influence of the baffle on the first natural frequency of the tank is significant.

As well known, the relationship between the excitation amplitude of the tank and the frequency of the maximum response (ω_1) is nonlinear. In this study, the frequency of maximum response of the baffled tank (ω_{b1}) under different excitation amplitudes (x_0=0.004d_0 and 0.01d_0), as illustrated in Fig.5, is analyzed and the results show that when ξ *<0.6,* the effect of different excitation amplitudes on ω_{b1} can be neglected. However, as ξ >0.6, both the excitation amplitude and the baffle height significantly influence the frequency of the maximum response of the baffled tank (ω_{b1}). The limitation of the present numerical model is at ξ=1, which the tank is divided into two half parts. Due to the limitation of Eq. 2.9, flow crossing over the baffle is not allowed. Based on the benchmark tests mentioned above, the results of the present numerical study are accurate. The proposed numerical method can be used to study the sloshing liquid in tanks with baffles.

3.2 Evolution of vortices and vortex shedding

As a viscous flow passes blunt bodies (baffles, screens, plate) in a tank, the generation of vortices and flow separation around the sharp corners of the internal structures are obviously seen. In this section, the evolution of vortices and the vortex shedding and the corresponding trajectory are discussed.

For liquid sloshing in a baffled tank, the vortices are developed near the tip of baffles. The correlation between the movement of baffles and sloshing liquid might be the clue to investigate the evolution of vortices around the baffle tip. Fig. 6 illustrates the wave history of point A and the displacement of tank for a tank excited at an excitation frequency of 1.0ω_1 with a baffle mounted on the middle of tank bottom. The excitation period of the tank motion T_e is 1.18s.

In the beginning of the excitation, the shear layer is generated around the baffle tip. As the wave sloshes from right to left (backward motion of the sloshing waves), the counterclockwise vortex (vortex M_1) appears on the left of the baffle tip (Fig. 7 (a)). On the contrary, as the wave sloshes from left to right (forward motion of sloshing waves), a clockwise vortex M_2 occurs on the right of the baffle tip (see Fig. 7 (b)). The occurrence of the vortices around the baffle tip is in connection with the formation of the separated shear layer and the distribution of horizontal pressure gradient ($\partial p / \partial x$). Besides, at the early transient period, vortices M_1 and M_2 are diminished by the forward and backward motion of the sloshing waves, respectively.

When the amplitude of sloshing waves increases, the vortices generated in the vicinity of the baffle tip grow in size. In the meanwhile, the vortex shedding occurs with the strong vertical jet on the sides of the baffle edge. The movement of the shedding vortices is primarily directed by the sloshing waves. The motion of the shedding vortex M_2 turns into moving in a northwest direction due to the backward movement of sloshing waves. Further, the strength and the size of the clockwise vortex M_2 are gradually reduced by the westward sloshing wave. Precisely, the upper and the lower parts of the clockwise vortex M_2 are suppressed and accelerated, respectively, by the westward moving flow. In addition, this accelerated stream passing the baffle tip results in the new counterclockwise vortex, whose strength is larger than the former counterclockwise vortex M_1. Vortex M_2 then almost disappears at $t = 3.92$ s at which another new vortex M_1 appears (Fig. 7 (c)). A nearly perfect round vortex occurs at $t = 4.24$ s (Fig.7(d)) at which the westward moving sloshing flow is almost ceasing. Note that the disappearing vortex M_2 remains some disturbance (see the square area in Fig.7(d)) to affect the ambient westward sloshing flow.

Soon after that, the sloshing flow starts moving eastward and the growth of counterclockwise vortex stops. The vortex becomes moving in a north-east direction and the size and the strength of the vortex are also reduced. Concurrently, the new clockwise vortex occurs at the right of the baffle tip and also grows to a perfect round vortex at $t = 4.88$ s (Fig. 7(e)) when the eastward sloshing flow ceases. In a very short period of time, the development of northwest jet just above the baffle tip against the counterclockwise circulation of vortex M_1 brings about the completely disappeared vortex M_1 at $t = 4.92$ s (Fig. 7 (f)).

Subsequently, the shedding vortex M_2 is not totally died out by the backward motion of sloshing flow. This is related to the size and strength of vortex M_2 which has evolved enough to resist the influence of the sloshing flow. Vortex M_2 continues to grow and interacts with the counterclockwise vortex M_1 after $t = 5.32$ s. The evolution of vortex shedding around the baffle tip and the movement of these vortices mentioned above constantly recur afterwards. Additionally, the flow pattern above the baffle tip illustrated in Figs. 7 (h) presents a snaky shape (see the square box in Fig. 7 (h)) which is caused by the co-exist dual vortices M_1 and M_2 with inverse circulation.

The snaky flow keeps moving upwards due to a vertical jet at the right hand side of the baffle and finally reaches the free surface. At t = 7.32 s, the head of the snaky flow impinges the free surface (see the subplot in Fig. 8 (a)) that partitions the flow near the free surface into two parts. Besides, the other clockwise circulatory flow appears on account of the interaction between the snaky flow and the free surface flow. The growth of the circulatory flow is, however, constrained by the earlier formed dual vortices and the backward sloshing flow. Subsequently, the wave sloshing backwards reduces the strength of vortex M_2 and so does the northeast jet (Arrow 2) between vortices M_1 and M_2. In the meantime, the northwest jet (Arrow 3) made by the snaky flow and vortex M_1 results in the growth of the nearly clockwise circulatory flow (vortex S_2) at t = 7.4 s. The clockwise vortex S_2 moves northwesterly and disappears very soon because of the backward motion of sloshing waves at t = 7.44 s. By the same token, the strength of vortex M_1 is reduced by another northwest jet (arrow 1) on the right of the baffle tip which decreases the strength of the northeast jet(arrow 2) and then vortex M_1 disappears at t = 7.44 s (Fig. 8(c)).

Hereafter, we name the major counterclockwise and clockwise vortices occurred at the baffle tip as vortices M_1 and M_2, respectively, and the secondary counterclockwise and clockwise vortices occurred away from the baffle tip as vortices S_1 and S_2. The above phenomenon repeat almost every 1.18s which is equal to the excitation period of the tank motion (T_e). The stronger and stronger interaction among major dual vortices, vertical jets and free surface flow results in the co-existence of the two secondary vortices, one is counterclockwise vortex S_1 and the other is clockwise vortex S_2, as shown in Figs. 8(d) and (e). At the later cycles, as illustrated in Fig. 9, the secondary vortices will spread in a wider region of the tank and even might reach the tank wall. As a result, there are three clockwise vortices coexist at the right side of the baffle (see Fig. 9(b)). The first major clockwise vortex (vortex M_2) is due to the shear layer along the baffle and the second clockwise vortex (new vortex S_4) is due to the interaction between the major vortex and the free surface, and the third vortex

S_2 comes from the second vortex departing from the snaky flow. Note that a small counterclockwise vortex (m_2) along the right wall of the tank is developed due to the interaction between the vortex S_2 and the shear layer along the right wall of the tank. Similarly, the same phenomenon mentioned above occurs on the left wall of the tank.

We will further discuss the trajectories of vortices. As mentioned above, the major vortices shed away from the baffle tip and move northeasterly or northwesterly due to the motion of the sloshing waves and then disappear. The flow beneath the free surface is influenced by the snaky flow and new vortices will be generated. The trajectories of the vortices M_1, M_2, S_1 and S_2 are depicted in Figs. 10 and 11. The vortex M_1 moves in a near clockwise direction. On the contrary, the clockwise vortex M_2 shows a counterclockwise movement (see Fig. 11(b)) and the trajectories of vortices M_1 and M_2 are correlated with the direction of sloshing waves. Further, as a tank is oscillated with a smaller excitation displacement of 0.002L, the trajectories of vortices depicted in Fig. 10(b) present that the moving distances of vortices are shorter than those shown in Fig. 10(a) with larger excitation displacement.

The hydrodynamic interaction between the snaky flow and the free surface flow creates vortices S_1 and S_2. As depicted in Fig. 11(c), the counterclockwise vortex S_1 and the clockwise vortex S_2 affected by the motion of sloshing flow move gradually to the left wall and (see Fig. 11(d)) to the right wall, respectively.

According to the detailed evolution of vortices in a baffled tank elucidated above, we may categorize the interaction process of vortices into four phases: A. Formation of separated shear layer and generation of vortices; B. Formation of a vertical jet and shedding of vortices; C. Interaction between shedding vortices and sloshing flow: the generation of snaky flow; D. Interaction between the snaky flow and sloshing waves. These four phases are separately discussed as follows.

A. Formation of separated shear layer and generation of vortices

During the very early period of excitation, the horizontal velocity (u) and the horizontal pressure gradient ($\partial p / \partial x$) at five vertical cross sections near the baffle tip are illustrated in Fig. 12. The location of the baffle centre is at X / L =0 and the thickness of the baffle is 0.01 L. The baffle height is 0.5 d_0 that indicates the submerged distance of the baffle top is - 0.25 m. The velocity vectors at t = 0.7 s, shown in the subplot of Fig. 12(a), indicate the baffle is moving rearward. The magnitudes of the horizontal velocity of five vertical cross sections are all positive. The shear layer just about the baffle tip is manifestly found (see X / L = - 0.005, 0, and 0.005) and the maximum horizontal velocity occurs on the right edge of the baffle tip (X / L = 0.005). The corresponding horizontal pressure gradients ($\partial p / \partial x$) of five vertical cross sections are depicted in Fig. 12(b) and the results show the negative pressure gradients predominantly distribute above the baffle tip. Note that the positive pressure gradient due to the backward motion of the baffle appears just under the right of the baffle tip (X / L = 0.01). The positive pressure gradient (adverse pressure gradient) at X / L = 0.01 will gradually force the flow to reverse its direction (right to left).

The baffle motion turns into a forward movement from t = 0.885 s to t = 1.475 s (see Fig. 6(b)). The distribution of the positive pressure gradient keeps extending and so does the strength of the negative horizontal velocity distribution. Additionally, the fluid particles near the right of the baffle tip encounters the forward motion of the baffle and this brings about an upward movement of the fluid particles. This phenomenon, therefore, intensifies the tendency of clockwise rotation of the flow. A clear flow separation on the baffle tip (X / L = 0 and 0.005) shown in Fig. 12 (e) also results in the occurrence of the clockwise vortex. Besides, the pressure gradient distributions in the vicinity of the baffle tip are all positive (see Fig. 12 (f)). Vortex M_2 is then vanished on account of the backward motion of sloshing waves. The forward motion of the baffle gradually affects the distribution of the pressure gradient nearby and a small negative pressure gradient is developed just at the centre of baffle top (X / L = 0), which is shown in Fig. 12 (h). The flow in the vicinity of the baffle tip will be forced to reverse its direction with the growth of the negative pressure gradient. Note that a northwest jet appears just near the right of the baffle tip depicted in the subplot of Fig. 12(g) and the development of the jet will be discussed later. The formation of the separated shear layer and the generation of vortex M_1 are similar to those of vortex M_2 and the detailed description of the M_1 formation is, therefore, omitted in the text

B. Formation of a vertical jet and shedding of vortices

As the sloshing displacement increases, vortices M_1 and M_2 grow in size and strength with time and a strong vertical jet will be developed which will force vortex M_1 or M_2 to shed away from the baffle. The occurrence of the strong vertical jet is followed by the vortex shedding phenomenon. Fig. 13 depicts the vertical velocity distribution at nine horizontal cross sections and the coordinate of the baffle top is at Y / L = -0.25. As shown in Fig. 13 (a), vortex M_2 is generated near the right of the baffle tip at t=3.3s. Soon after, a clear vertical jet illustrated in Fig. 13 (b) is formed at the right hand side of the baffle and this growing vertical jet finally interrupts the link between the baffle and vortex M_2 and then vortex M_2 sheds away from the right edge of the baffle. In the same way, as illustrated in Fig. 13(c), the vertical jet is also created on the left of the baffle tip by the counterclockwise vortex M_1. After t = 4.3s (Fig. 13 (c)), the vortex M_1 is shed away from the baffle by the effect of the vertical jet. In order to estimate the shedding frequency of vortices around the baffle tip, we further define a new Reynolds number (R_{EB}) in relation with the vertical velocity on the left or right of the baffle tip.

$$\mathrm{R}_{EB} = \frac{V_b \times d_0}{\upsilon}, \quad V_b = \frac{v_{tip} \times d_0}{d_0 - d_b} \tag{3.2}$$

where v_{tip} is the vertical velocity of the mesh above the right edge of the baffle tip ((X/L, Y/L) =(-0.005,-0.245)). The time history of R_{EB} presented in Fig. 14 (a) unearths a periodic state after t =

20s. In addition, the enlarged plot of R_{EB} from $t = 3$ s to 7 s is depicted in Fig. 14 (b). The solid and dashed lines are corresponding to the generation of vortices M_1 and M_2, respectively. Furthermore, the major peaks of R_{EB} are corresponding to the generation of vortices M_1 and M_2, whereas the minor peaks of R_{EB} are related to the vortex shedding. The power spectral density analyses based on Welch's method [20] of R_{EB} with various excitation frequencies are depicted in Fig. 15(a). The results illustrated in Fig 15(a) show the occurrence of two dominant peaks, one is the excitation period of the tank (T_e) and the other is a half of the T_e that represents the vortex shedding period. For a baffled tank excited at a frequency of $1.0\omega_1$ with various d_b/d_0, the results of the power spectral density analyses of R_{EB} is depicted in Fig. 15(b) and the baffle height has limited influence on the period of vortex shedding. The vortex shedding period is, therefore, primarily dominated by the excitation period of the tank and is nearly equal to $T_e / 2$.

Fig. 16 depicts the instantaneous streamlines of a baffled tank excited at $1.0\omega_1$ with various baffle heights. The vortex shedding frequencies shown in Fig. 16 are between 0.58s and 0.6s and are almost equal to a half of the frequency of external forcing. Again, the vortex shedding frequency is independent of various baffle heights. For a baffled tank excited at different excitation frequencies, the instantaneous streamlines are illustrated in Fig. 17. The vortex shedding frequencies demonstrated in Fig. 17 are close to $T_e/ 2$. As described above, the vortex shedding phenomenon is strongly correlated with the strength of the vertical jet in the vicinity of the baffle tip. When the external forcing frequencies are far away from the first natural mode of the baffled tank (ω_{b1}), both the strength of sloshing flow and the vertical jet decrease and no vortex-shedding phenomenon appears.

C. Interaction between shedding vortices and sloshing flow: the generation of snaky flow

As dissected in Figs. 8, the formation of snaky flow stems from the interaction between the shedding vortices and the sloshing flow. The snaky flow are formed by the jets between the vortices. These jets play an important part to influence the generation of the secondary vortices S_1 and S_2. The wide range of horizontal velocity distribution at eleven vertical cross sections between X / L = -0.1 and 0.1 is demonstrated in Fig. 18. As depicted in Fig. 18(a), a snake-like velocity distribution is presented. Additionally, there are three flow separations that implies the coexisting of three vortices: two clockwise vortices and one counterclockwise vortex. The twists of the velocity profile can be correlated with four jets. In other words, the snaky flow is mainly composed by four jets (see Fig. 18 (b)) : Jet 1 : is formed by the interaction between the clockwise flow of vortex M_2 and the baffle; Jet 2: the northeast jet that appears between vortex M_1 and vortex M_2 by the interaction between them; Jet 3: the northwest jet due to the interaction between vortex M_1 and the clockwise vortex S_1 ; Jet 4: the northeast free surface flow is driven by clockwise vortex S_2. . The directions of four jets mentioned above depend on the circulation of vortices and the direction of sloshing flow. The direction of snaky flow, therefore, varies with time on account of the interaction among vortices and sloshing flow. Further, the phenomenon of free surface flow partitioned into two parts by the northwest jets (Jet 3) and Jet 4 of the snaky flow is presented in Fig. 18 (a) and also can be found in Figs. 18 (e) and (f) (see the velocity distribution in the square). As shown in Figs. 18 (c) and (d), the intensities of Jet 1 and Jet 3 are increased by the backward motion of sloshing flow, whereas, those of Jets 2 and 4 are reduced because of the inverse direction among Jets 2 and 4 and the sloshing flow. The similar phenomenon occurs when the wave sloshes from left to right, which is shown in Figs. 18 (e) and (f).

D. **Interaction between snaky flow and sloshing waves**.

The consequence of the interaction between the snaky flow and sloshing waves is the occurrence of vortices S_1 and S_2. The jets among vortices and the free surface are the main sources contributing to the generation of vortices S_1 and S_2 (see Fig. 8.) Figs. 19 (a) and (b) further illustrate the horizontal velocity distribution related to the combination between vortices M_1 and S_1 (see Figs. 20 (a) and (b)). By comparing to the direction of Jet 4, the opposite twists depicted in Fig. 19 (a) beneath the free surface (see the square) indicate the existence of vortex S_1. At t = 8.52 s, the combination of vortex M_1 and vortex S_1 occurs (see Fig. 20 (b)) and enlarges the maximum horizontal velocities (X / L = 0.05 and 0.07) almost 1.5 times of those at t=8.48s shown in Fig. 19 (a). As demonstrated in Figs. 19 (c) and (d), the similar phenomenon occurs when vortex S_2 is merged with vortex M_2 (see Figs. 20 (c) and (d)) and the maximum horizontal velocities (X / L = 0.05 and 0.07) at t = 9.16 s increase nearly twice as large as those at t = 9.08 s (Fig. 19 (c)).

3.3 Relationship between vortex size and baffle height

We continue to explore the scale of the vortices generated around the baffle tip for a tank with various heights of the baffles. The parameters of liquid depth = 0.3 L and excitation frequency = $1.05\omega_1$ are used in this section. As depicted in Fig. 21, we denominate the absolute horizontal distance between the baffle center and the vortex center is $\mathbf{V_{Lx}}$ and the vertical distance from the vortex center to the baffle tip is $\mathbf{V_{Ly}}$**.** That is, $\mathbf{V_{Lx}}$ and $\mathbf{V_{Ly}}$ are the location of the vortex centre referring to the baffle tip. $\mathbf{V_w}$ and $\mathbf{V_h}$ represent, respectively, the width and the height of the vortex. Fig. 22, only illustrates the streamlines of the cases of the baffle heights = 0.1, 0.5 and 0.8d_0, though, eight different baffle heights are used in the simulations. To neglect the influence of the other shedding vortices, the vortices around the baffle tip are measured before the occurrence of flow separation. Since the vortices will be generated in either the left or the right hand side of the baffle, the size of the vortices is determined by averaging the sizes of the vortices occurred on the either left or right corner of the baffle during one cycle of the tank motion.

The results of the dimensionless size of vortices are listed in Table 1 and shown in Fig. 23. The maximum horizontal coordinate of the vortex center ($\mathbf{V_{Lx}}$ $/d_0$ = 0.141) occurs as ξ = 0.2 and the minimum one appears at ξ = 0.8 and so does $\mathbf{V_{Ly}}$ $/d_0$. For all the other cases, the magnitudes of $\mathbf{V_{Lx}}$ $/d_0$ are between 0.1 and 0.12 (see Fig. 23 (a)). As shown in Fig. 23 (b), the width of the vortices

(V_w/d_0) enlarges with the increase of baffle height when $\xi \leq 0.5$ and is the largest at $\xi = 0.5$ and diminishes with the growth of baffle height afterward. The height of the vortices (V_h/d_0) increases as does baffle height until $\xi = 0.65$, whereas, it decreases as baffle height increases afterwards. Further, the height of vortices (V_h/d_0) are larger than the width of the vortices (V_w/d_0) when $\xi > 0.2$. This implies that the vortices grow dominantly in the vertical direction as $\xi > 0.2$.

Fig. 24 shows the horizontal and vertical velocities distribution of the selected baffle heights and the absolute maximum horizontal and vertical velocities of vortices versus various baffle heights are illustrated in Fig. 25. As shown in Fig. 25, the maximum and the minimum horizontal velocities of vortices appear at $\xi = 0.2$ and 0.8, respectively, that implies the biggest and the smallest V_{Lx} / d_0 accordingly. The variation of the vertical coordinate of the vortex center (V_{Ly} / d_0) is insignificant by comparing with V_{Lx} / d_0 that indicates the vortex center mostly travels in the horizontal direction before the occurrence of vortex shedding. Additionally, the maximum V_{Ly} / d_0 also occurs at $\xi = 0.2$.

The variation of the sizes of vortices under various baffle heights mentioned above can be correlated with the velocity distribution of vortices by examining the maximum horizontal and vertical velocities of the vortices shown in Fig. 25. When $\xi \leq 0.2$, the increases of both the maximum horizontal and vertical velocities of the vortices depicted in Fig. 25 demonstrate the size of the vortices intensifying with the growth of baffle height. Besides, the size of the vortex as $\xi \leq 0.2$ dominantly develops in the horizontal direction rather than in the vertical direction because the increasing rate of the horizontal velocity of the vortex is larger than the vertical velocity of the vortex. In other words, the vortices created near the baffle tip are effortless to touch the tank bottom and then grow along the tank bottom when the baffle height is small.

3.3.1 Vortex shedding with various baffle height

The development of the vortex shedding for $\xi = 0.1$, which is slower than those for larger baffle height. The fact is correlated with the strength of the vertical jet for $\xi = 0.1$ is evolved slowly.

As shown in Fig. 24, the vertical jet of ξ = 0.1 at t = 5.775s (Fig. 24 (b)) is smaller than those of d_b/d_0 = 0.5 at t=3.325. Further, the velocity distribution illustrated in Fig. 24 demonstrates that the negative horizontal velocities of the vortices are always larger than those of positive ones. The reason is trivially that the flow on the upper half of the vortex is free to circulate, whereas, that on the lower half is blocked by the baffle. Similarly, the positive vertical velocities of the vortices are always larger than those of negative ones due to the formation of the vertical jet along the baffle walls.

The maximum vertical velocity of vortices presented in Fig. 25 is always larger than the maximum horizontal velocity of vortices except for a small region near ξ = 0.2. The strength of the vortices, therefore, predominantly intensifies vertically. That is, as the baffle height enlarges, the vortices are free to grow vertically along the baffle walls until those vortices touch the tank bottom.

The width and the height of the vortices start to reduce when $\xi > 0.5$ and $\xi > 0.6$, respectively, as shown in Fig. 23(b). The variation of the sizes of the vortices mentioned above indicates the growth of vortices in the horizontal direction is restrained by the baffle height when $\xi > 0.5$ and, similarly, the vertical growth of vortices is limited when $\xi > 0.6$. In other words, the considerable damping effect caused by the larger baffle height on the sloshing waves will affect the evolution of vortices around the baffle tip. On the other hand, the strength of sloshing flow decreases as well because ω_{b1} of the tank gradually shift away from the excitation frequency with the growth of the baffle height. Thus, the maximum vertical velocity of vortices illustrated in Fig. 25 also reduces as $\xi > 0.5$.

3.3.2 Vortex shedding and liquid depth

The streamline of selected times of ξ = 0.2, 0.5, 0.8 and 0.95 are presented in Fig. 26 and the streamline patterns demonstrate obviously the phenomenon of vortex shedding. As the ratio ξ is close to 1 (see Fig 26(d)), the gap between the end of baffle top and the free surface is small and, therefore, the space for vortices growing is limited. In addition, the vortex-shedding phenomenon only occurs when the excitation frequency of the tank is close to the lowest natural mode (ω_{b1}) of the baffled tank. As depicted in Fig. 26(d), the vortices mainly grow in the horizontal direction due to the suppression of the free surface on the vertical growth of the vortices. The shedding vortices move horizontally along the free surface and then gradually travel to the both ends of the tank walls. Additionally, the vortices keep shedding from the baffle tip and interact with the earlier shedding vortices. As shown in the figure, the apparent three vortices link together along the free surface at t =12.28 s. The sloshing amplitude and the resonant modes will be influenced by these eddies due to the consequence of energy dissipation.

With the excitation displacement x_0= 0.004L, baffle height = 0.5d_0, and excitation frequency ω_x =1.05ω_1, the influence of water depth on the evolution of vortices around the baffle tip is shown in Fig. 27 and the corresponding sizes of the vortices are listed in Table 2. The magnitude of $\mathbf{V_{Lx}}$ decreases as the water depth increases. In addition, the difference between $\mathbf{V_{Lx}}$ and $\mathbf{V_{Ly}}$ also decreases as the water depth increases. In other words, the vortex center predominantly moves horizontally when d_0 / L is equal to 0.3 before the occurrence of vortex shedding. As the water depth increases, the vertical movement of the vortices becomes more obvious. Further, the height of the vortex (V_h) increases with the growth of liquid depth, whereas, the width of vortexices (V_w) seems to be independent of the influence of water depth. The baffle height might be the key effect to restrict the horizontal growth of the vortices.

3.3.3 Evolution of vortex during transient period

We continue to utilize the cases demonstrated in Fig.27 to elucidate the evolution of vortices in the transient period under different water depths. The process of the generation of vortices in the transient period has been mentioned in section 3.2. The interval between the baffle tip and the free surface is varied with various liquid depths and the evolution of vortices might be different as well. Fig. 28 depicts the streamlines of a baffled tank with d_0/L =0.3, 0.5, and 0.7. The linkage of the vortices just beneath the free surface is clear-cut when d_0/L =0.3 (Fig. 28(a)). This reveals that the vortices shedding from the baffle tip interact easily with the vortices appearing near the free surface due to the interaction of the snaky flow and sloshing waves and the interaction will restrict the growth of the free surface vortices. Further, the free surface vortices of d_0/L=0.7 are much larger than those of d_0/L=0.3. The gap of d_0/L =0.3 between the baffle top and the free surface is smaller comparing to those of d_0/L =0.5 and 0.7 and the shedding vortices, therefore, are more effortless to interact with the other vortices just beneath the free surface.

When d_0/L =0.5 and 0.7, as shown in Figs. 28 (b) and 28 (c), two larger vortices appear just beneath the free surface and they can be referred to vortices S_1 and S_2 as mentioned in section 3.2. The vortices developed on the both side of bottom corners of the baffle clearly occur during the transient period when d_0/L = 0.3. However, this phenomenon becomes unobvious during the transient stage when d_0/L = 0.5 and 0.7. Besides, the evolution of the vortices near the bottom corners of the baffle not only occurs earlier but becomes stronger with the decrease of liquid depth. The generation of the vortices near the bottom corners of the baffle is in connection with the formation of boundary-layer separated flow. The water depth, therefore, might be the key effect of the flow separation around the bottom corners of the baffle.

3.3.4 Evolution of vortices during steady state

As the size of the vortices created adjacent to the bottom corners of the baffle grows, the interaction among these vortices is significant, especially, the hydrodynamic interaction among the vortices is more visible during the transient period when d_0/L = 0.3. We believe that the interaction among vortices is also correlated with the liquid depth of the tank. The evolution of the vortices during the steady state is then explored as follows. Fig. 29 depicts the instantaneous streamlines of a tank with d_0/L = 0.3 in the steady-state period. After t >100 s, the time history of sloshing displacement presents a steady-state oscillation and therefore, we may assume the sloshing waves are in a steady state. As depicted in Fig. 29, a new born clockwise vortex (M_2) is formed at the right of the baffle tip at t =100.48s and a clear secondary counterclockwise vortex (S_1) at the west-north direction of the baffle remains and is about $0.2d_0$ away from the baffle tip. At the same time, the former minor clockwise vortex (m_1) at the left side of the baffle wall does not completely vanish. As the major vortex M_2 grows (see Fig. 29 (b)), the secondary clockwise vortex S_1 sinks downward very soon and interacts with the former minor vortex m_1 and also with the bottom shear layer at the left baffle corner. Then, this reorganizes the clockwise vortex m_1 and produces a counterclockwise vortex m_3 right beneath vortex m_1. Vortex S_1 almost occupies the left part of the tank and does not vanish during the steady state. Besides, a new secondary counterclockwise vortex S_2 occurs at the north-east direction of the baffle and the horizontal distance between vortex S_2 center and the baffle tip is also about 0.2 d_0. About 0.04s later, vortex S_2 sinks down and moves toward the right corner of the baffle and a strong vertical jet appears along the baffle which forces vortex M_2 to shed away from the baffle tip. Note that another newborn clockwise vortex m_2 next to S_2 appears at t =100.8s (Fig. 29 (c)) and it disappears very soon at t =100.88s (Fig. 29 (d)) due to interacting with vortex S_2. In addition, a minor vortex m_5 is generated near the left wall of the tank by the separated shear layer along the wall. The size of vortex M_2 grows differently from that in the transient period at which vortex M_2 keeps growing with a size larger than that of the steady state and might dance with the former counterclockwise vortex M_1 born at 0.5 excitation cycle earlier. In other words, the size of vortex M_2 in the steady state is much smaller than that in the transient period and vortex M_2 is destroyed by the backward sloshing flow soon after it sheds from the baffle tip at t =101.16 s (Fig. 29 (g)). Almost at the same time, a new vortex M_1 occurs at the left of the baffle tip but its growth is constrained by the continuously growing vortex m_1 and vortex S_1 with nearly a constant size. Although vortex S_1 keeps pressing vortex m_1, no vertical jet can be created at the left side of the baffle since the counterclockwise flow is blocked by the clockwise vortex m_1. The interaction of vortices S_1 and m_1 generates a strong northeast stream which forces vortex M_1 to leave the baffle tip with the forward motion of sloshing flow. From t =101.24 s to 101.4 s (Figs. 29 (h)-(j)), the N-E stream interacts with the snaky flow that reorganize the nearly dying vortex M_2 and vortices M_1 and M_2 are dancing as a pair of tadpoles. Besides, vortex m_2 recurs next to vortex S_2 and a new vortex m_4 appears at the right wall of the tank due to the separated shear layer along the wall. Vortex m_2 again disappears rapidly and so dose vortex m_4. Note that the north-east stream passing over the baffle tip creates a downward fall along the right side of the baffle and vortex S_2 forced by this downward fall moves upward. Vortex S_2 merges vortex M_2 and they are destroyed by the forward motion of sloshing flow immediately and finally vortices M_1, M_2 and S_2 disappear at t = 101.56s (Fig. 29 (l)) at which ends one evolution cycle of streamline pattern during the steady state.

As d_0 increases to $0.5L$ and the baffle height to $0.25L$ ($0.5d_0$), Fig. 30 shows the streamlines of a complete cycle during the steady state. At t =101.36s (Fig.30 (a)), a new M_2 is generated at the right of the baffle tip and the bowl type of streamline pattern near the free surface appears. In the meanwhile, as depicted in Fig. 30 (a), a secondary vortex S_2 and a minor vortices m_2, m_3, m_4 exist. Only 0.12s later (see Fig. 30 (b)), the free surface stream becomes weaker and weaker and the bowl-like streamline pattern shifts to a un-even pair of counter-clockwise vortices, S_1 and S_3, which are formed by the interaction of former incompletely dying vortex M_1 and the snaky flow. The snaky flow is enhanced by Jet 1 generated by the combined effect of vortices M_2 and S_2. Strong southwest downward flow at the right of vortex S_2 due to the back motion of sloshing flow forces it to lift up and vortex S_2 then destroys vortex M_2 with the sloshing flow from t =101.48s to 101.66s (Figs. 30 (b)-(d)). Concurrently, the snaky flow impinges the free surface resulting in a separated flow and the left stream of the separated flow is stronger than the right one due to the movement of sloshing flow. Vortex S_1 is then sunk down by the left flow. Further, two minor vortices, m_2 and m_4, reduce in size from t=101.48s to 101.66s and reorganize after t=101.96s (Fig. 30 (e)) because of the interaction of the movement of sloshing flow and vortex S_2. Another bowl-like streamline pattern formed by vortex S_2 and the backward movement of sloshing flow appears at t=101.96s (Fig. 30 (e)) and a new vortex M_1 is generated. The interaction of vortices M_1 and S_1 forces S_1 to sink down. Only 0.12s later (Fig.

30 (g)), the combination effect of vortices S_1 and m_1 and the forward motion of sloshing flow creates a upward Jet 2 which forces vortex M_1 to shed away from the baffle tip and the streamline pattern at t =102.16s (Fig.30 (g)) is nearly symmetrically to that at t=101.6s (Fig.30 (c)).

As described early, the hydrodynamic interaction among vortices is different for a baffled tank with various liquid depths. Thus, a brief investigation of the evolution of vortices in the shallow water depth (d_0/L = 0.1) is presented in Figs. 31 and 32 during the transient and the steady-state periods, respectively. The complicated interaction among vortices is noticeably seen during both the transient and the steady-state periods. In addition, the vortex generated around the right of baffle tip from t = 101.84 s to t = 102s (Figs. 32 (a)-(d)) grows vertically upwards and the height of the vortex is almost equivalent to the liquid depth.

The stories of the evolution of vortices described above are just a few examples and it is important to realize that the growth and the hydrodynamic interaction of the vortices sensitively depend on the baffle height, liquid depth, excitation frequency of the tank, and excitation displacement. Any alteration of one of the conditions listed above would make the occurrence of another different story related to the vortices evolution.

4. Conclusion

The numerical study and experimental measurement of liquid sloshing in a 2D tank with a vertically tank bottom-mounted baffle are demonstrated and discussed. The fictitious cell approach is used to deal with the fluid-structure domain near the baffle tip. Both the convergence study of the present numerical model and the benchmark tests show a good accuracy of the computational results. The comparison between the experimental measurement and the numerical results validates again the consistency of the present numerical simulations. Comprehensive investigations, including the evolution of vortices and vortex shedding phenomenon due to baffles, the relationship between the vortex shedding frequency and the excitation frequency of the tank, the vortex size generated in the vicinity of the baffle tip, the interaction of vortices inside the tank, are elucidated in detail and the following key conclusions are made:

.

1. The evolution of vortices inside a baffled tank in terms of vortex generation, vortex shedding and the trajectories of vortices are analyzed and the interaction processes are categorized into four phases: A. Formation of separated shear layer and generation of vortices; B. Formation of a vertical jet and shedding of vortices; C. Interaction between shedding vortices and sloshing flow: the generation of snaky flow; D. Interaction between the snaky flow and sloshing waves.
2. The vortex shedding phenomenon in the vicinity of the baffle tip is tightly correlated with the strength of the vertical jet along the baffle walls and the excitation frequency of the tank. Vortex shedding phenomenon due to stronger vertical jets occurs when the excitation frequency is close to the first natural mode of the baffled tank (ω_{b1}).
3. The size of the vortex generated near the baffle tip is discussed and the vortex size is closely correlated with the baffle height. When the baffle height is small ($d_b \leq 0.2\ d_0$), the vortex size mainly grows in the horizontal direction. Instead, the vortex size dominantly develops in the vertical direction as $d_b \geq 0.3\ d_0$.
4. The period of the generation and shedding of vortices near the baffle tip is nearly about one half of the excitation period of the tank. The coupled effect of the excitation frequency of sloshing flow and that of external forcing might be the factor that the shedding frequency of vortices is not exactly equal to $T_e / 2$. Consequently, the frequency of vortex shedding in the baffled tank is apparently dominated by the external forcing frequency.
5. The disappearance of the vortex shedding phenomenon occurs when the external forcing frequencies are far away from the first natural mode of the baffled tank (ω_{b1}) due to the weakly influence of the vertical jets.
6. The evolution of vortices is closely related to the growth and the hydrodynamic interaction of the vortices and sensitively depends on the baffle height, liquid depth, excitation frequency of the

tank, and excitation displacement.

Acknowledgement

The first author would like to profoundly thank Prof. Faltinsen's supervision during his short term study in NTNU, Norway. This study is partially supported by a grant NSC-100-2221-E-110-007.

Reference

[1] P. Banerji, M. Murudi, A. H. Shah, N. Popplewell, Tuned liquid dampers for controlling earthquake response of structures, Earthquake Engineering and Structural Dynamics, 29(2000) 587-602

[2] P. Banerji, A. Samanta, S. A. Chaban, Earthquake vibration control of structures using tuned liquid dampers: experimental studies, International Journal of Advanced Structural Engineering 2(2) (2010), 133-152.

[3] L.M. Sun, Y. Fujino, B.M. Pacheco, P. Chaiseri, Modeling of tuned liquid damper (TLD), Journal of Wind Engineering and Industrial Aerodynamics, 43(1–3)(1992) 1883-1894

[4] D. Reed, J. Yu, H. Yeh, S. Gardarsson, Investigation of tuned liquid dampers under large amplitude excitation, Journal of Engineering Mechanics, 124(4)(1998) 405–413.

[5] Y. Fujino, L. Sun, M.B. Pacheco, P. Chaiseri, Tuned liquid damper (TLD) for suppressing horizontal motion of structures,. Journal of Engineering Mechanics, 118(10)(1992) 2017–2030.

[6] M. Marivani, S. Numerical simulation of structure response outfitted with a tuned liquid damper, Computers and structures, 87(2009) 1154-1165.

[7] C. G. Koh, S. Mahatma, and C. M. Wang., Theoretical and experimental studies on rectangular liquid dampers under arbitrary excitations, Earthq. Engrg. Str. Dynam., 23(1994) 17-31.

[8] Y. Kim, Numerical simulation of sloshing flows with impact loads, Appl. Ocean Res. 23(2001) 53-62.

[9] Y., Kim, Y.S., Shin, K.H. Lee, Numerical study on sloshing-induced impact pressures on three-dimensional prismatic tanks, Appl. Ocean Res. 26(2004) 213-226.

[10] P. Warnitchai, T. Pinkaew, Modelling of liquid sloshing in rectangular tanks with flow-damping devices, Eng. Struc. 20(1998)593-600.

[11] M Isaacson, S. Premasiri, Hydrodynamic damping due to baffles in a rectangular tank, *Can.* J. Civ. Eng. 28(2001) 608-616.

[12] O.M. Faltinsen, and A. N. Timokha, Sloshing. Cambridge University Press (2009).

[13] J.R. Cho, H.W. Lee, Numerical study on liquid sloshing in baffled tank by nonlinear finite element method, Comput. Meth. Appl. Mech. Eng. 193(2004) 2581-2598.

[14] J.R. Cho, H.W. Lee, Free surface tracking for the accurate time response analysis of nonlinear liquid sloshing, J. Mech. Sci. Technol. 19(2005) 1517-1525

[15] K. C. Biswal, S. K. Bhattacharyya , P. K. Sinha, Non-linear sloshing in partially liquid filled containers with baffles, Int. J. Numer. Meth. Engng. 68(2006) 317-337.

[16] D. Liu, and P. Lin, Three-dimensional liquid sloshing in a tank with baffles, Ocean Eng. 36(2009) 202-212.

[17] R. D. Firouz-Abadi, H. Haddadpour, M. A. Noorian, M. Ghasemi, A 3D BEM model for liquid sloshing in baffled tanks, Int. J. Numer. Meth. Engng. 76(2008) 1419-1433.

[18] P. K. Panigrahy, U. K. Saha, D. Maity, Experimental studies on sloshing behavior due to horizontal movement of liquids in baffled tanks, Ocean Eng. 36(2009) 213-222.

[19] C. Lin, T. C. Ho, S. C. Chang, S. C. Hsieh, K. A. Chang, Vortex shedding induced by a solitary wave propagating over a submerged vertical plate, Inter. J. Heat and Fluid Flow, 26(2005) 894-904

[20] P. A. Berthelsen, O. M. Faltinsen, A local directional ghost cell approach for incompressible viscous flow problems with irregular boundaries, J. Comp. Phys. 227(2008) 4354-4397.

[21] B.F. Chen, R. Nokes, Time-independent finite difference analysis of fully non-linear and viscous fluid sloshing in a rectangular tank, J. Comput. Phys. 209(2005) 47-81.

[22] B.F. Chen, Viscous free surface effects on coastal embankment hydrodynamics, Ocean Eng. 26 (1999) 47–65.

[23] C. H. Wu, B. F. Chen, Sloshing waves and resonance modes of fluid in a 3D tank by a time-independent finite difference method, *Ocean Eng.* 36(2009) 500-510.

[24] C. H. Wu, O. M. Faltinsen, B.F. Chen, Numerical study of sloshing liquid in tanks with baffles by time-independent finite difference and fictitious cell method, Comput. Fluids 63(2012) 9-26.

[25] B.F. Chen, and C.H. Wu, Effects of excitation angle and coupled heave–surge–sway motion on fluid sloshing in a three-dimensional tank, J Mar Sci Technol.16(2011) 22–50.

[26] P.D. Welch, The Use of Fast Fourier Transform for the Estimation of Power Spectra: A Method Based on Time Averaging Over Short, Modified Periodograms, IEEE Transactions on Audio Electroacoustics, AU-15(1967), 70–73.

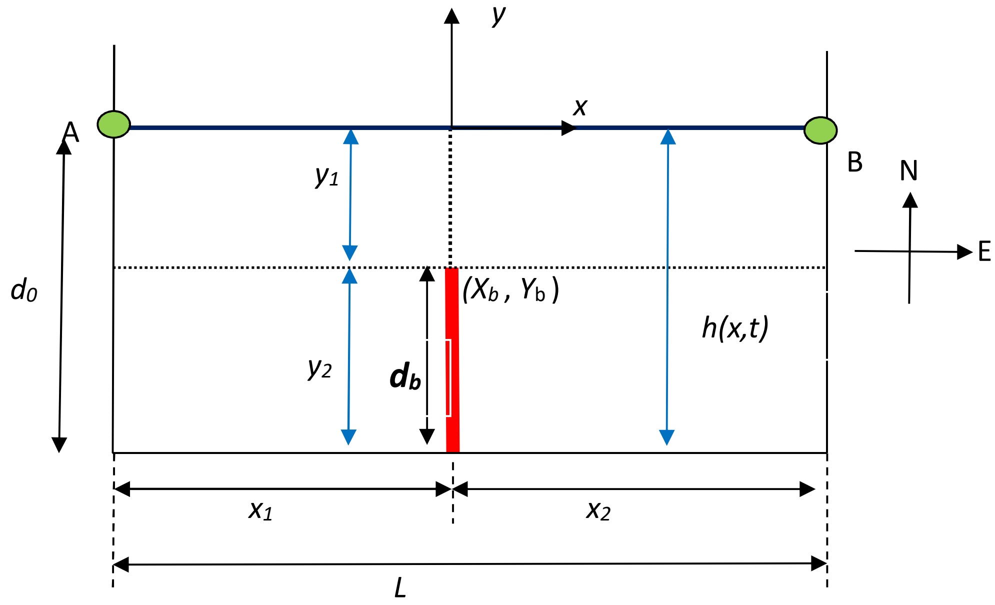

Fig. 1 The new coordinate transformation on the tank with a tank bottom-mounted baffle

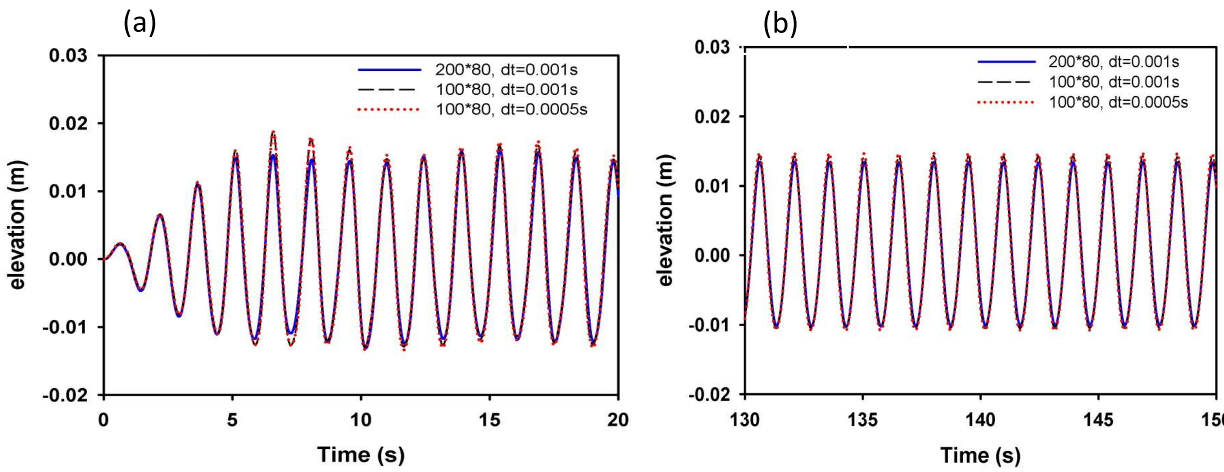

Fig. 2 The convergence study for a vertically tank bottom-mounted baffle. The wave elevation at left wall of the tank. (a) the transient period; (b) the steady-state period. d_0/L=0.5, d_b/d_0=0.75, x_0/L=0.002, ω_x=0.8ω_1 (ω_1 is the first natural mode of the partially filled tank).

(a)

(b)

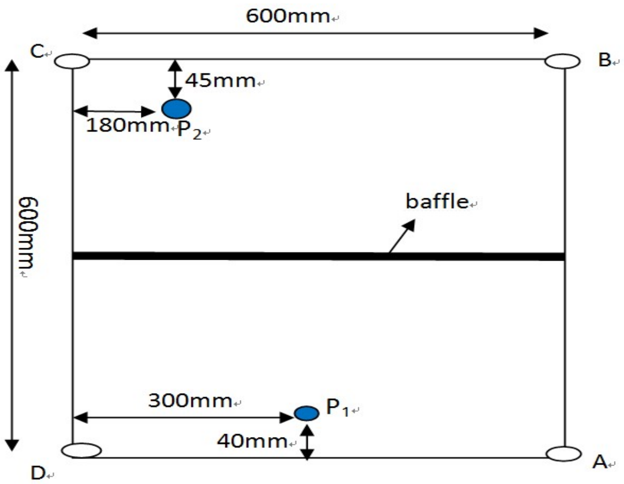

Fig. 3 (a) Photograph of the experiment setup of a baffled tank; (b) positions of the wave probes (P1, P_2) from the top view of the baffled tank. Measurements in mm

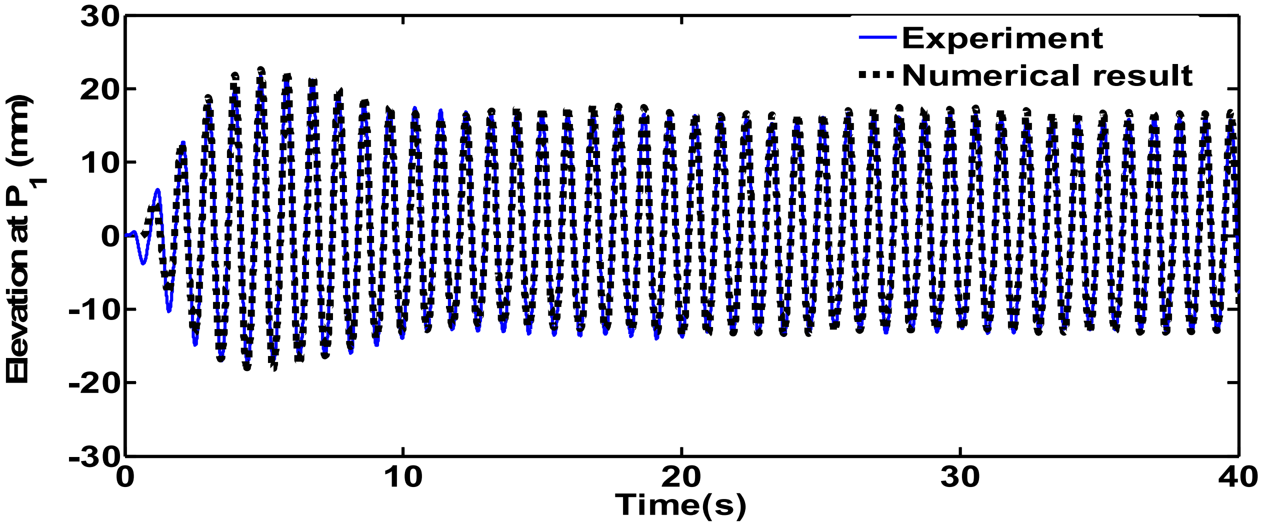

Fig. 4 The comparison of wave elevation at Probe P_1 between the experiment and numerical simulation in a baffled tank under surge motion. d_0/L=0.5, d_b/d_0=0.5, x_0/L=0.004, ω_x=1.0ω_1

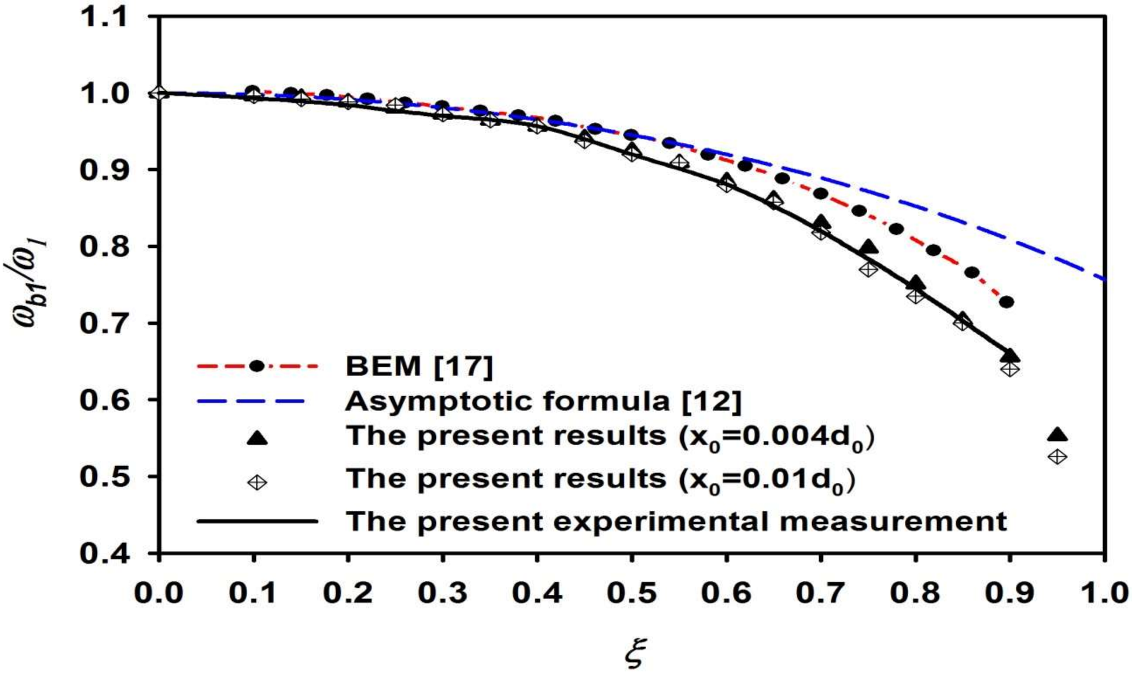

Fig. 5 The non-dimensional lowest natural frequency (ω_{b1} / ω_1) versus baffle height-to-liquid depth $\xi = d_b/d_0$ for a vertically tank bottom-mounted baffle at the middle point with the liquid depth-to-tank height d_0/L =0.5. ω_{b1}: the lowest natural frequency of the baffled tank

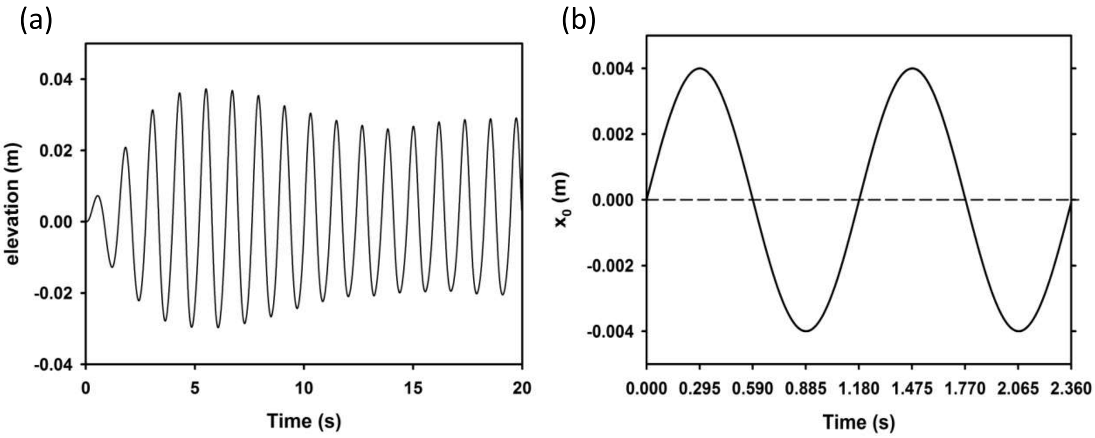

Fig. 6 (a) the wave history of point A and (b) the tank displacement for a tank with a vertically baffle mounted on the tank bottom. d_0 / L=0.5, d_b / d_0 =0.5, x_0 / L=0.004, L=1m. ω_x =1.0ω_1.

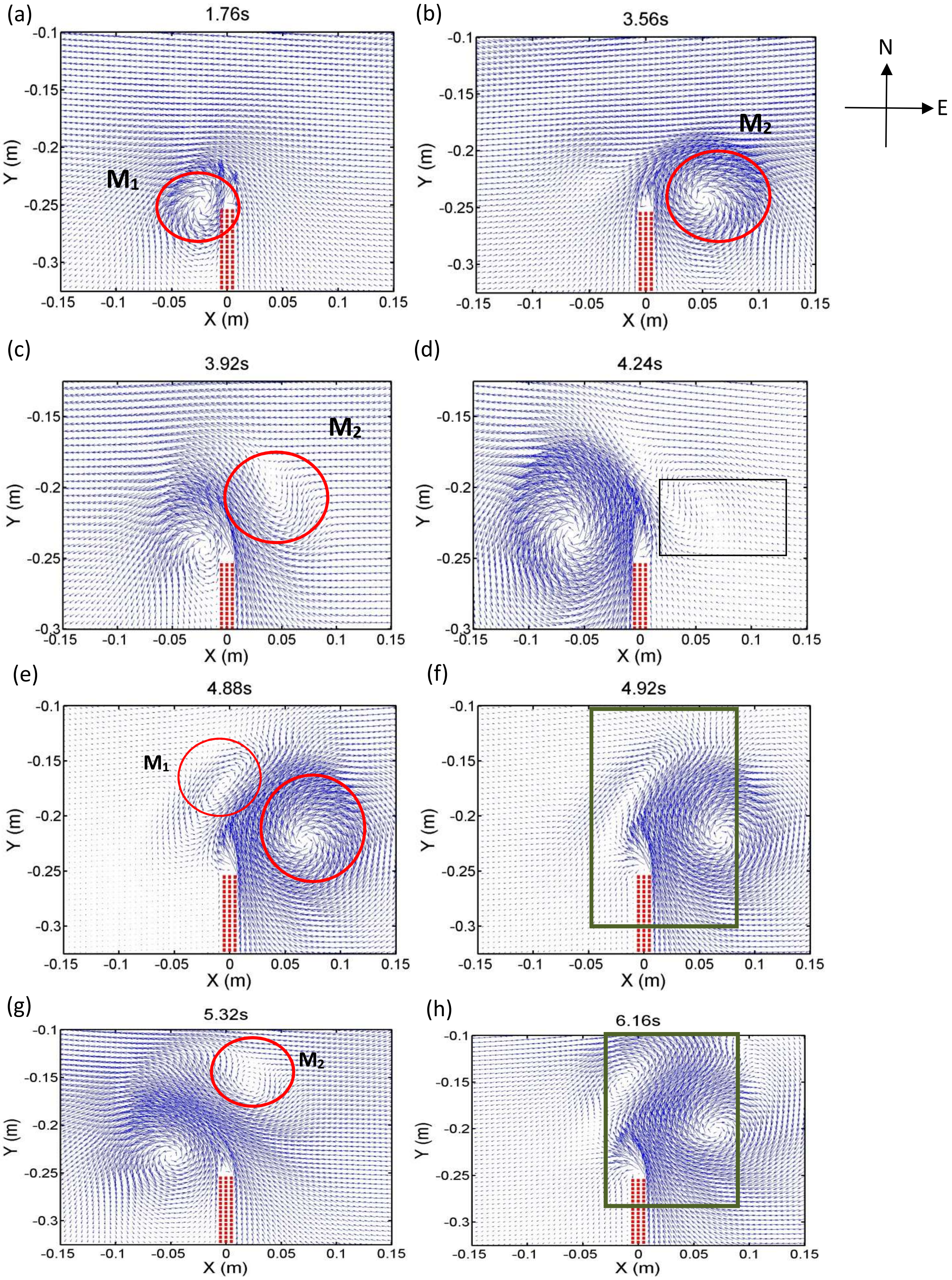

Fig. 7 Velocity vectors for a tank with a bottom-mounted baffle. The baffle-tank geometry and tank motion is the same as in Fig. 6.

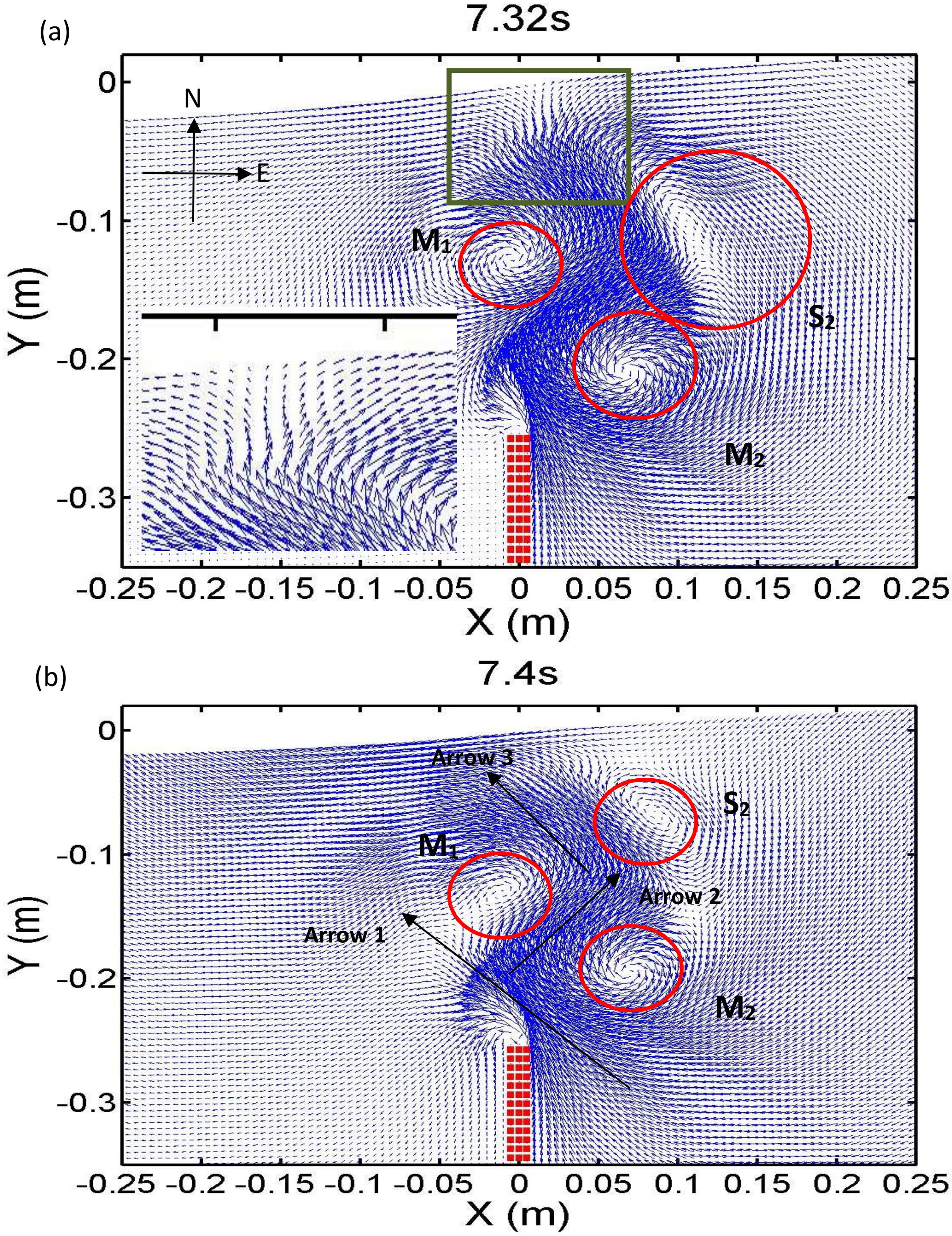

Fig. 8 Velocity vectors for a tank bottom-mounted baffle. The baffle-tank geometry and tank motion is the same as in Fig. 6.

(c)

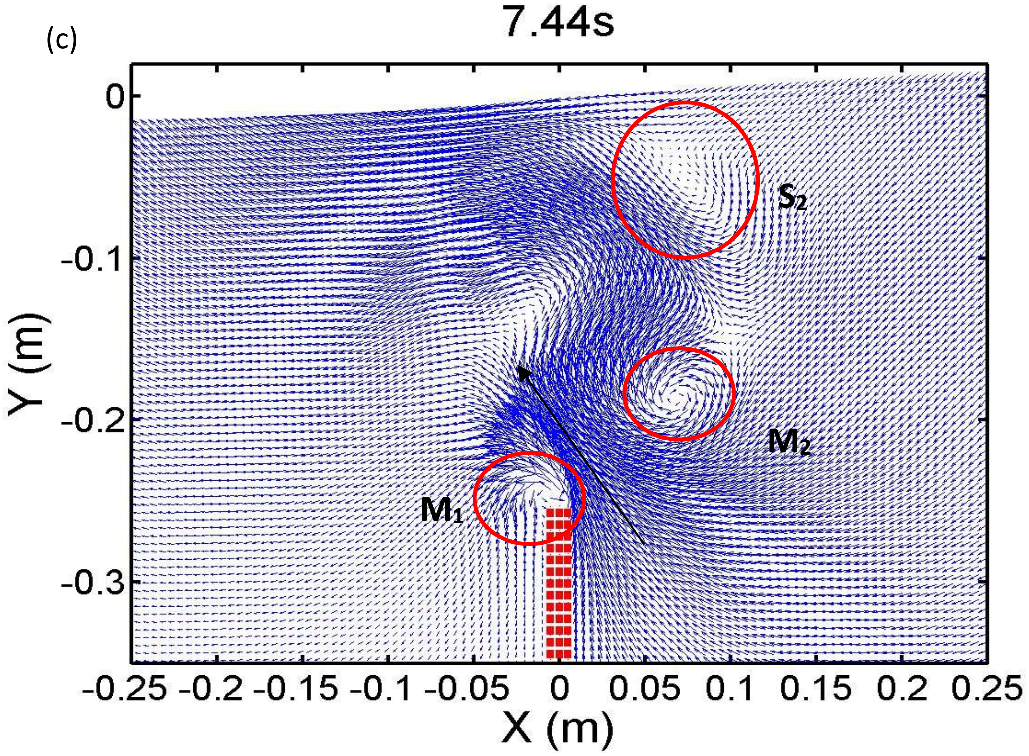

(d)

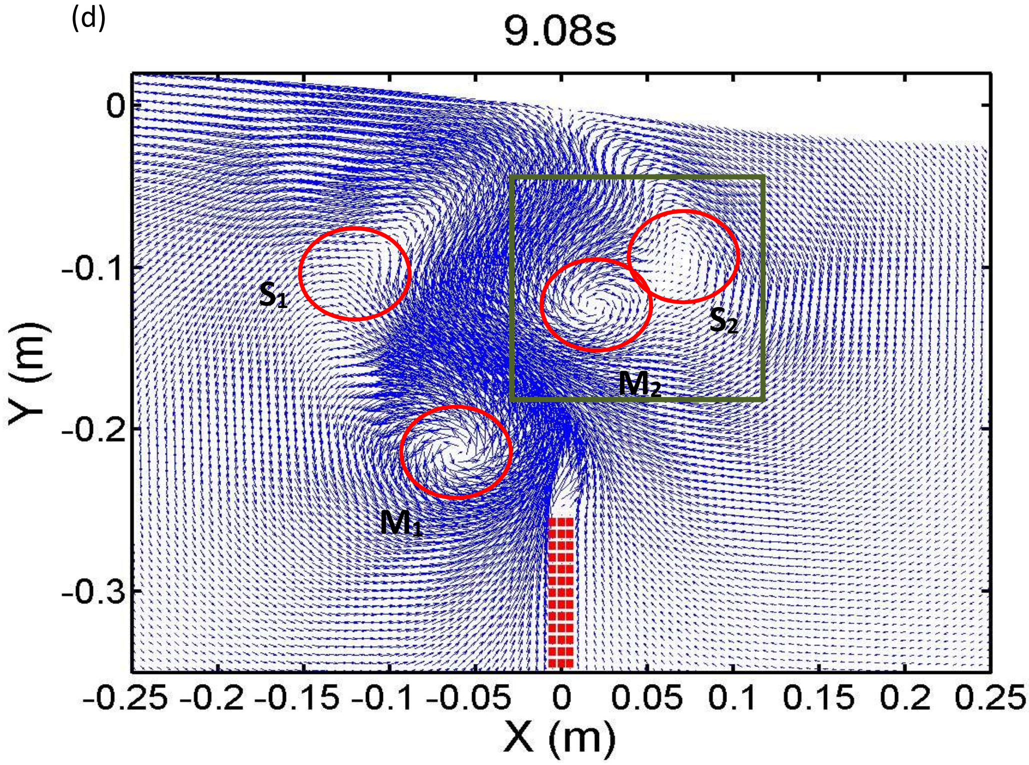

Fig. 8 Continued

(e)

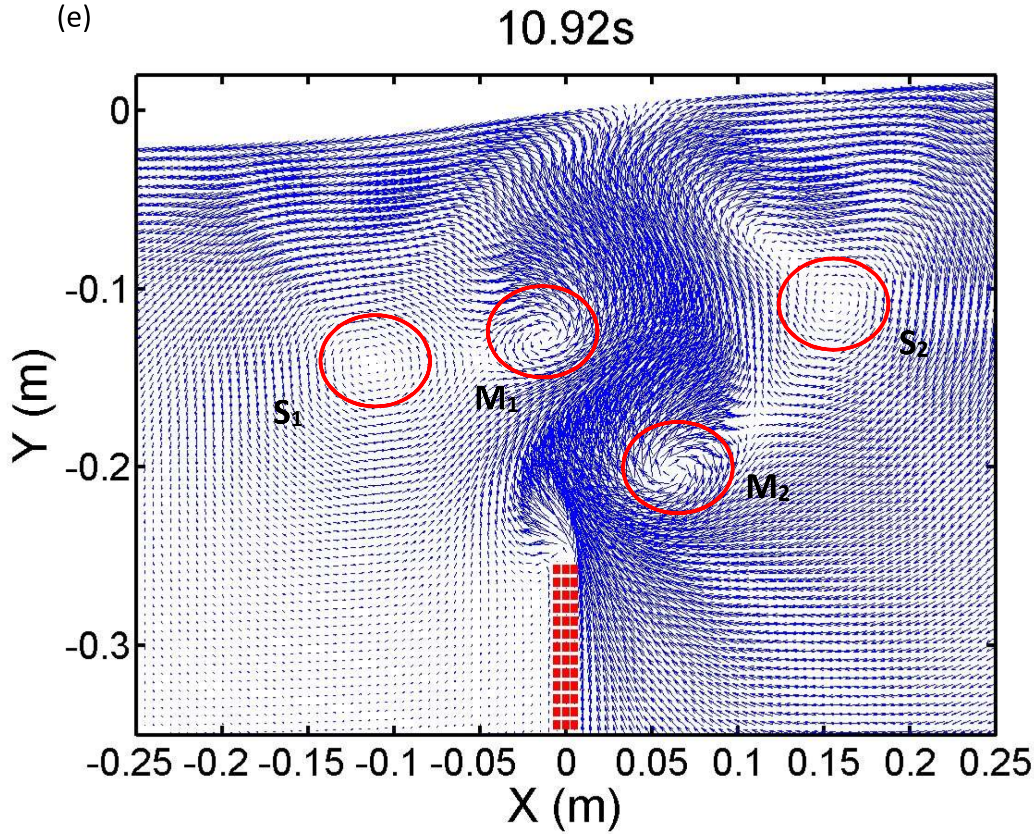

Fig. 8 Continued.

(a)

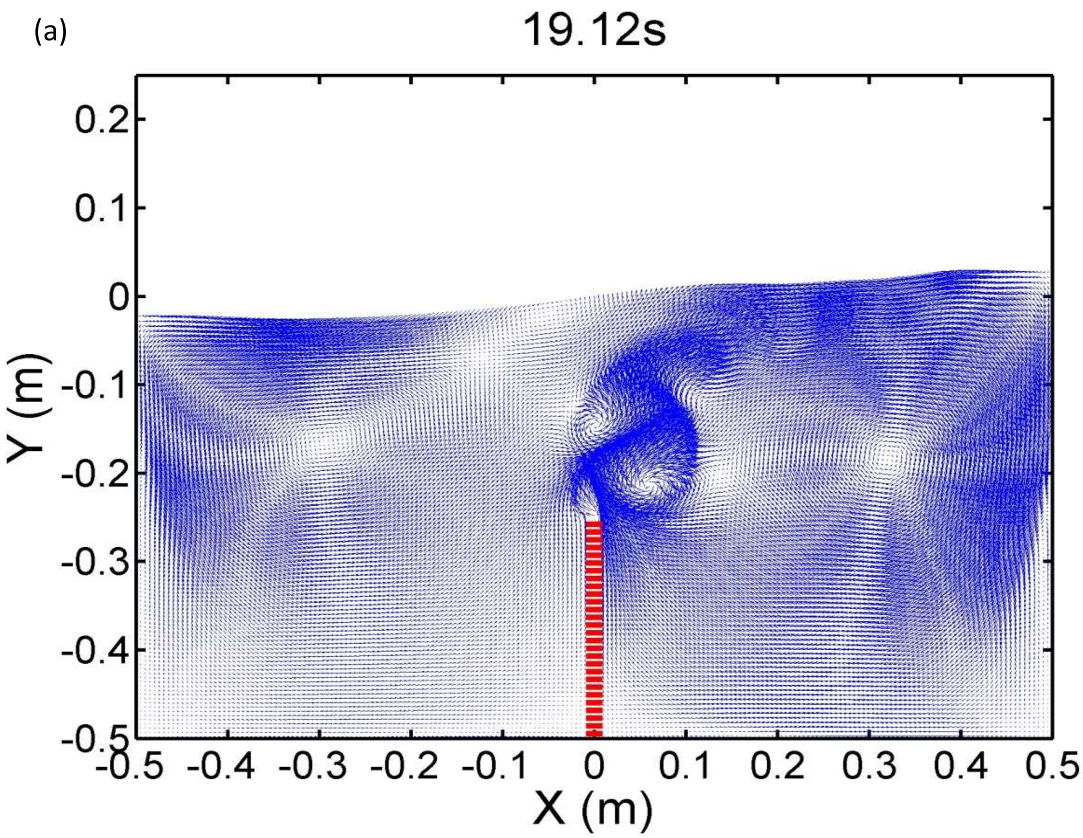

(b)

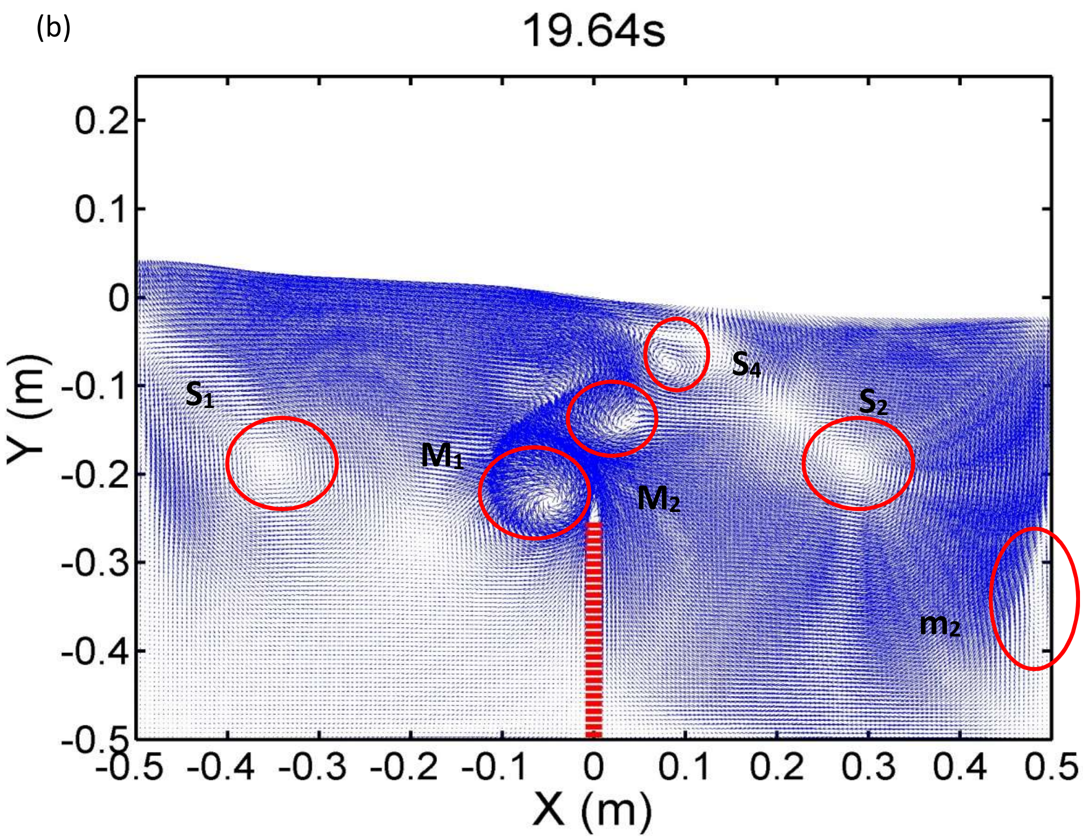

Fig. 9 The flow field of liquid sloshing in a tank with a vertically bottom-mounted baffle. The baffle-tank geometry and tank motion is the same as in Fig. 6.

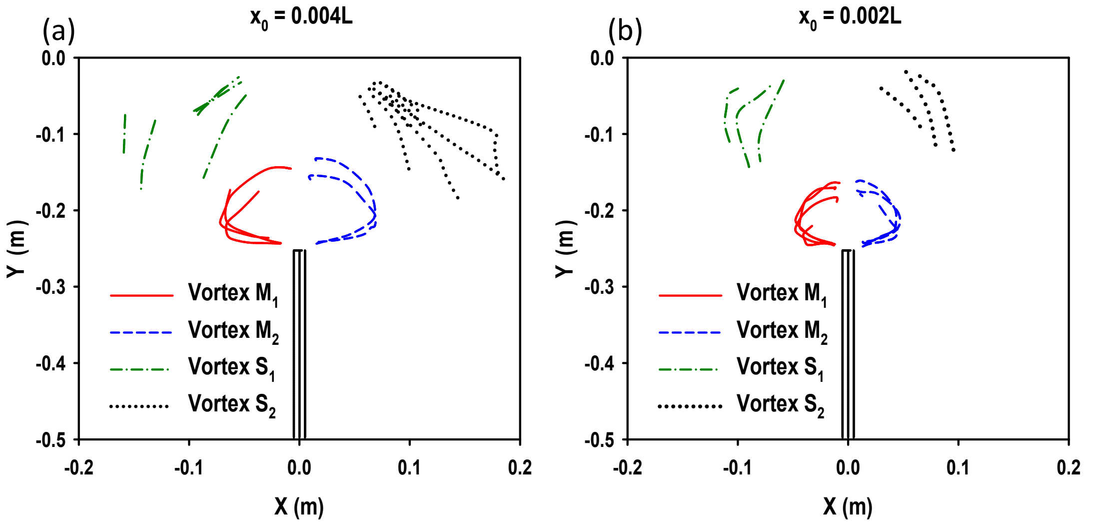

Fig. 10 The trajectories of vortices. The baffle-tank geometry and tank motion is the same as in Fig. 6

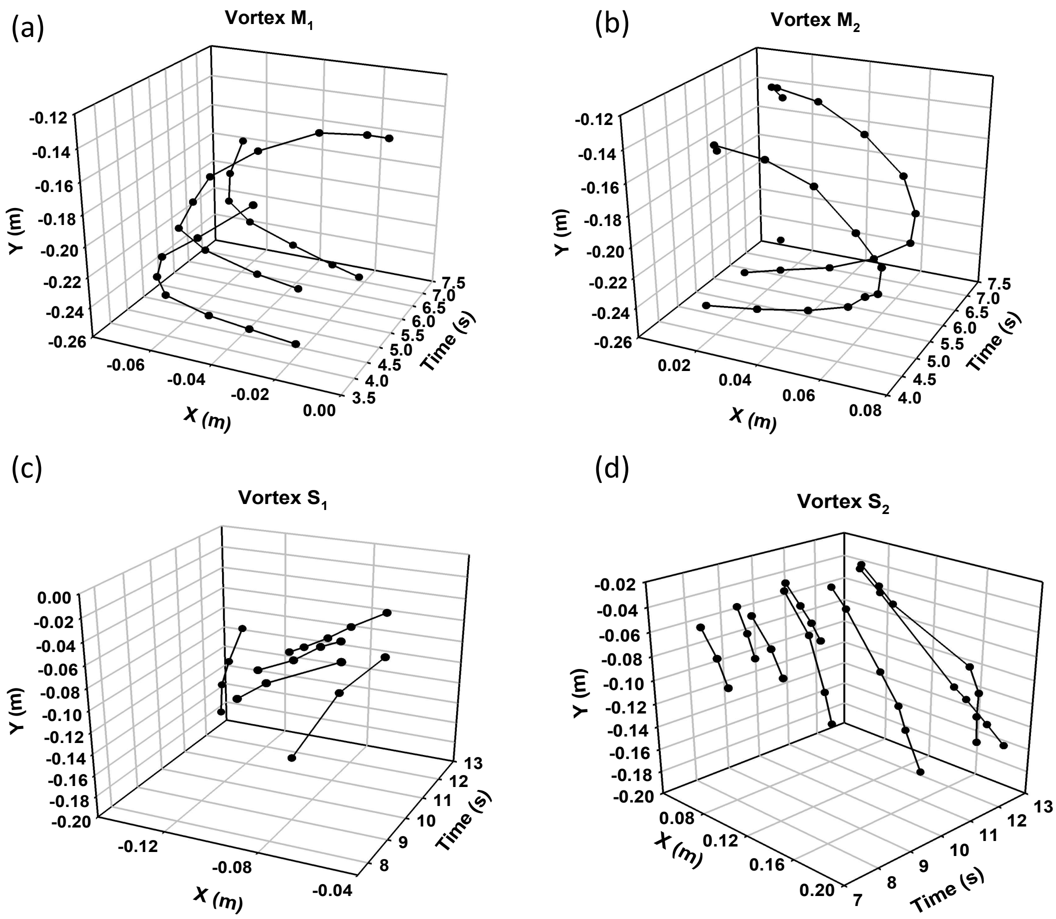

Fig.11 The time history of the trajectories of the vortices M_1, M_2, S_1, and S_2.

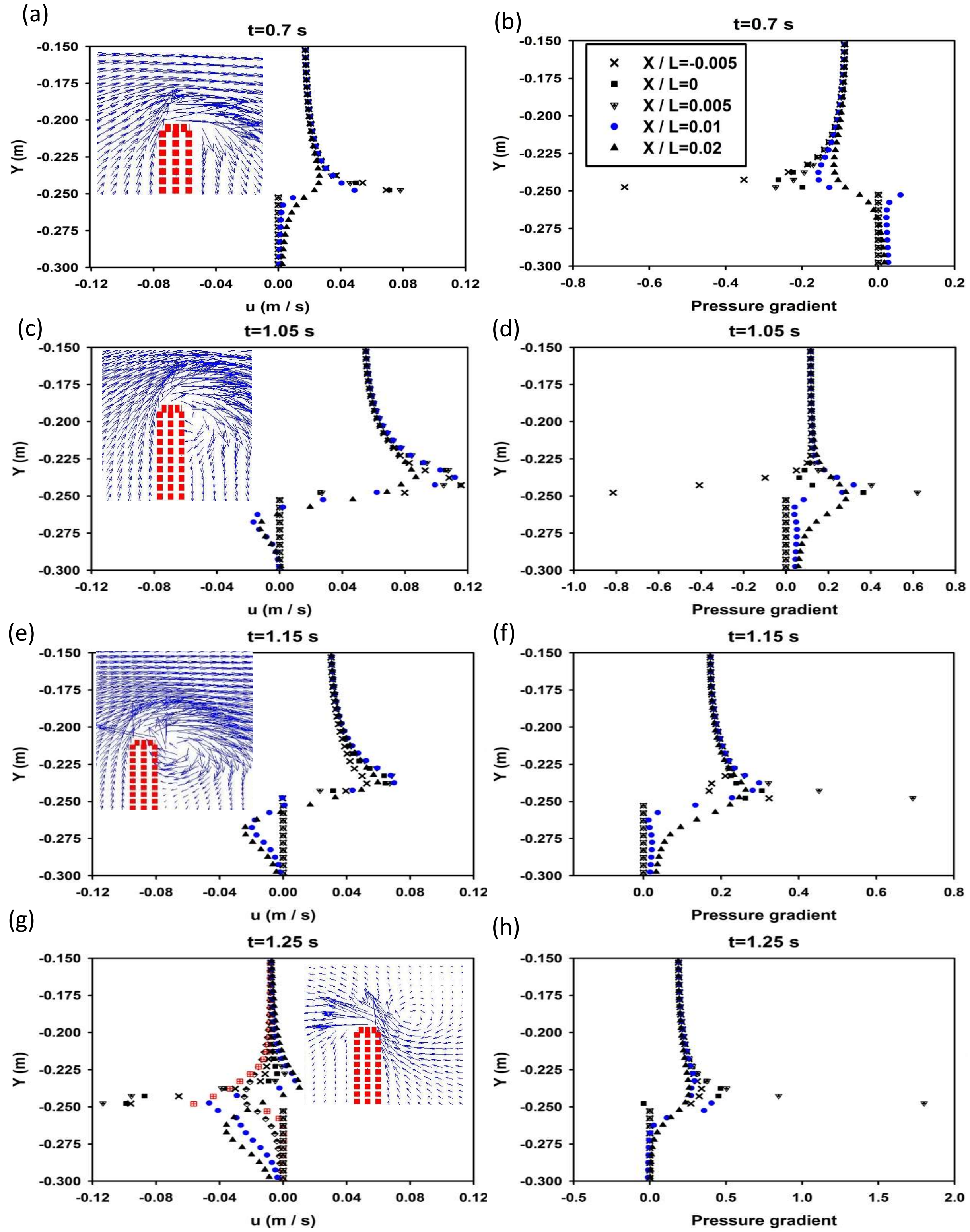

Fig. 12 Variation of the horizontal velocity distribution and the horizontal pressure gradient at five vertical cross sections between X / L = -0.02 and 0.02. The insert depicts the velocity vectors around the baffle tip.

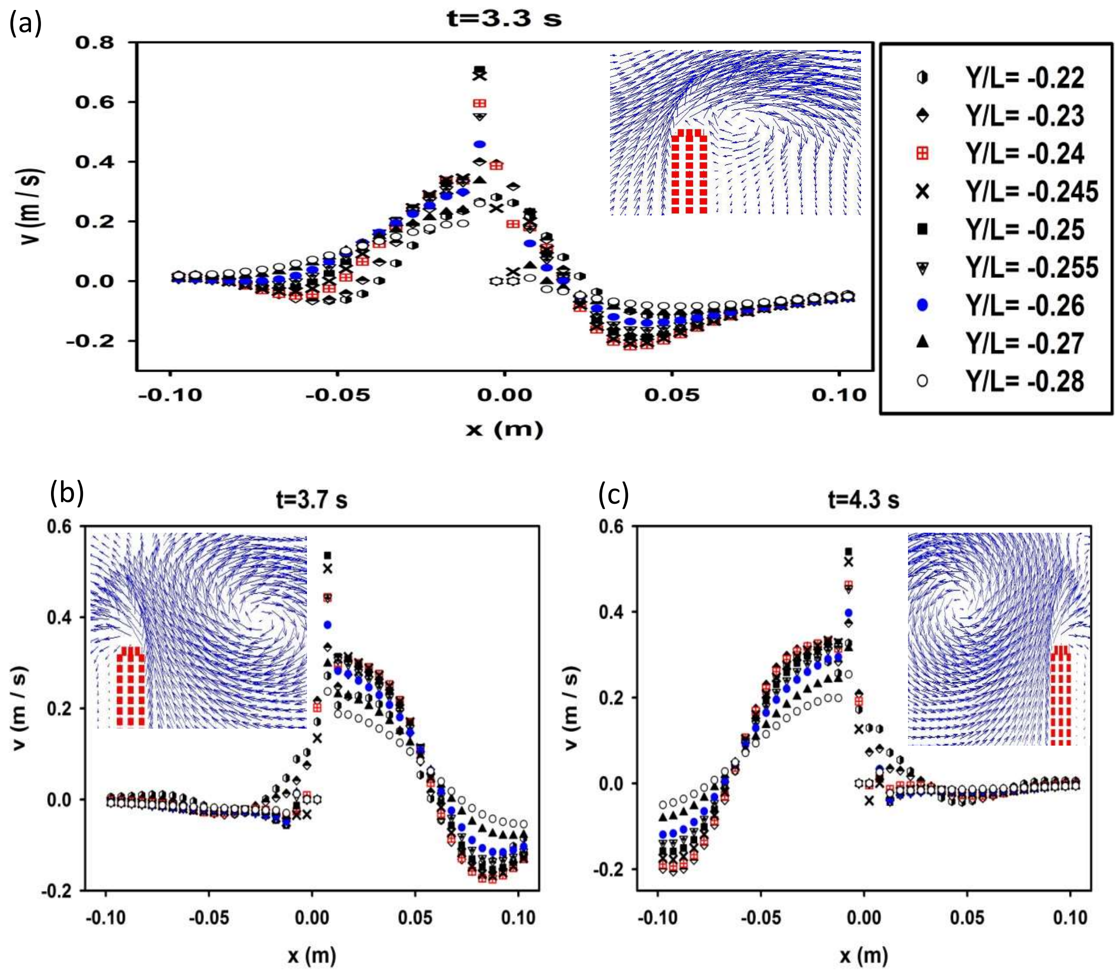

Fig. 13 Variation of the vertical velocity distribution at nine horizontal cross sections between Y / L = -0.22 and -0.28. The insert depicts the velocity vectors around the baffle tip.

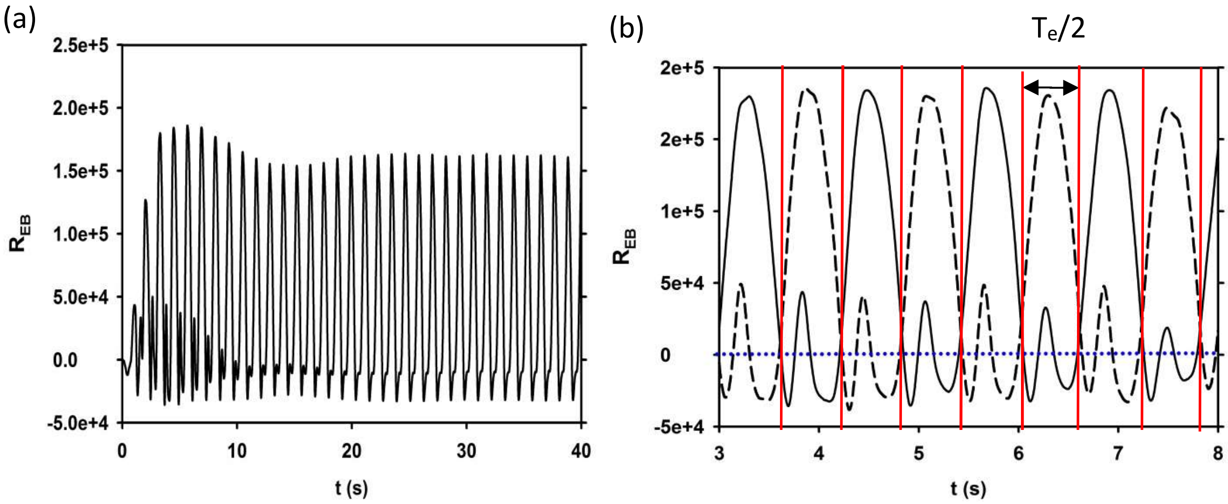

Fig. 14 The time history of Reynolds number (R_{EB}). (a) R_{EB} of v_{tip} at (X/L, Y/L)=(-0.005,-0.245) (b)solid line: R_{EB} of v_{tip} at (X/L, Y/L)=(-0.005,-0.245) and dash line: R_{EB} of v_{tip} at (X/L, Y/L) =(0.005,-0.245) T_e: the excitation period of the tank. The baffle-tank geometry and tank motion is the same as in Fig. 6.

(a)

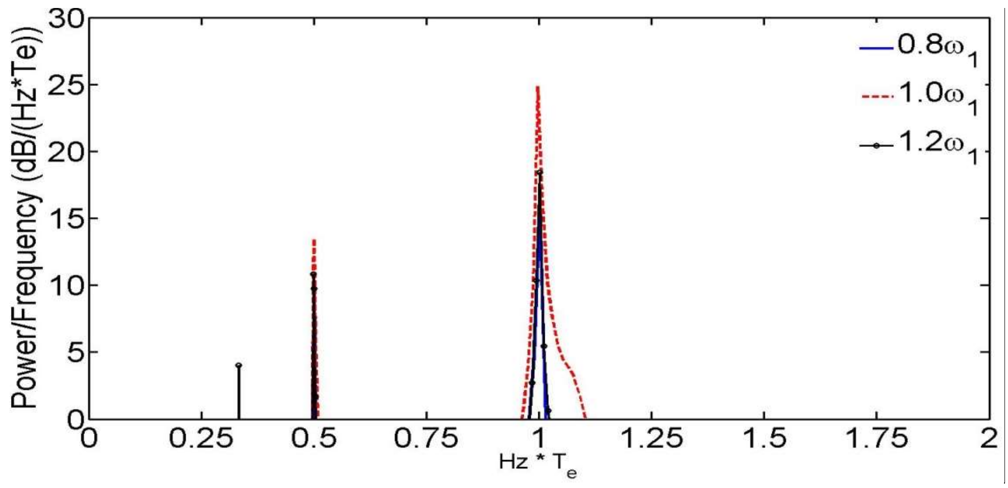

(b)

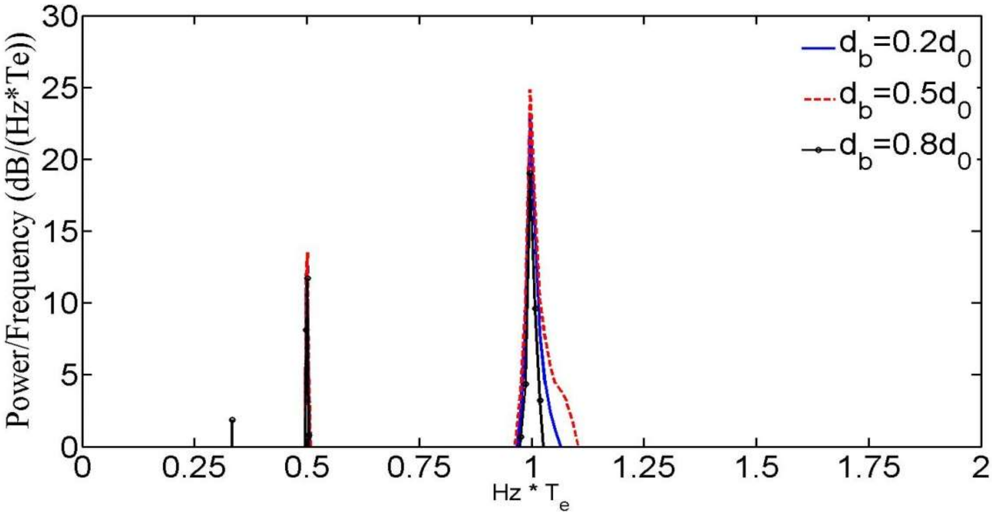

Fig. 15 The PSD (power spectral density) analyses of R_{EB} for a 2D baffled tank (a) excited at various excitation frequencies, d_b/d_0=0.5, x_0/L=0.004; (b) with different baffle heights, ω_x =1.0ω_1 , x_0/L=0.004.

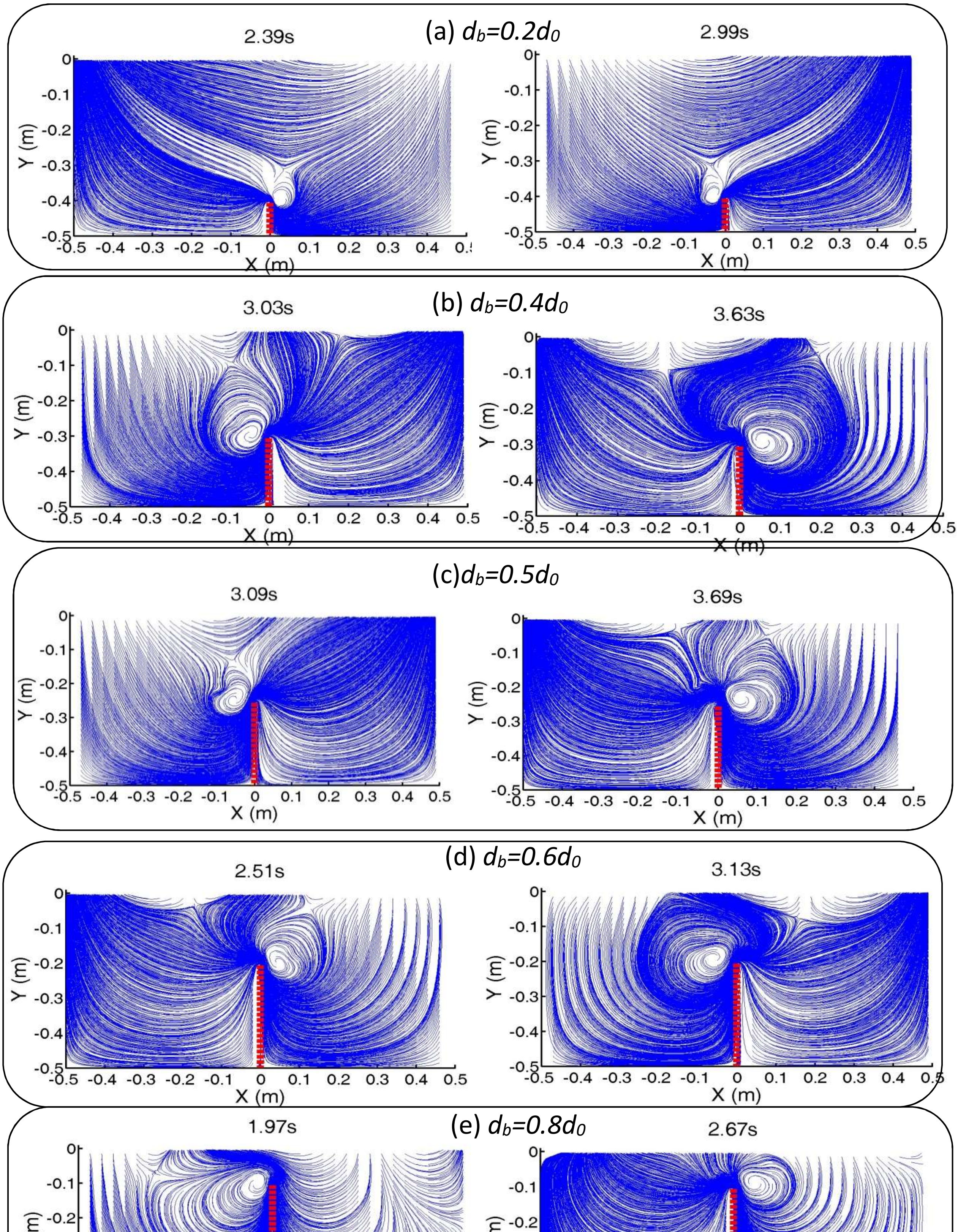

(a) $d_b=0.2d_0$
2.39s
2.99s
(b) $d_b=0.4d_0$
3.03s
3.63s
(c) $d_b=0.5d_0$
3.09s
3.69s
(d) $d_b=0.6d_0$
2.51s
3.13s
(e) $d_b=0.8d_0$
1.97s
2.67s
Y (m)
X (m)

Fig. 16 Streamline plots of vortex shedding for a tank with various baffle heights (d_b). $d_0\,/\,L$=0.5, $x_0\,/\,L$=0.004, L=1m. ω_x=1.0ω_1

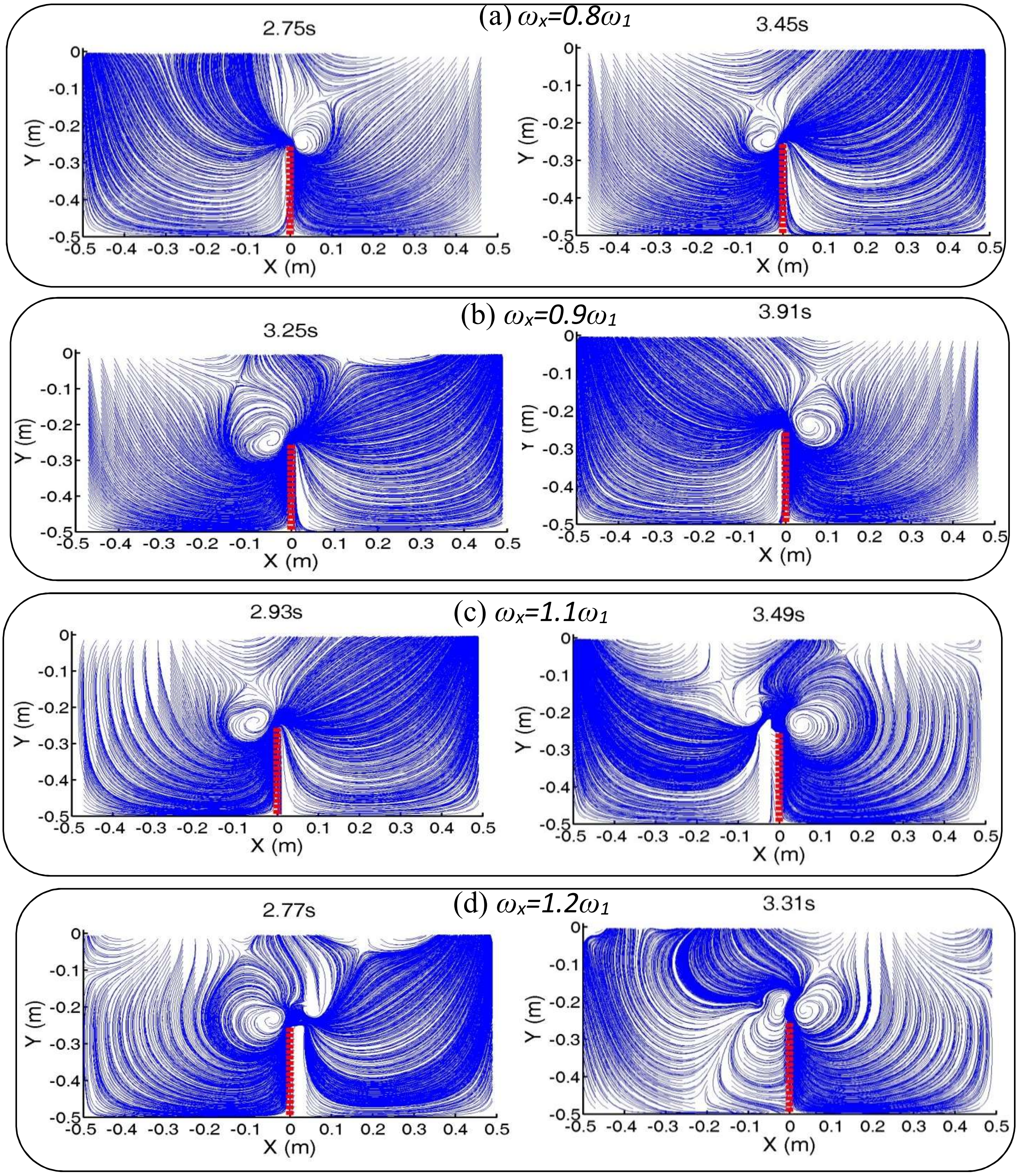

Fig. 17 Streamline plots of vortex shedding for a baffled tank with various excitation frequencies. $d_0\,/\,L$=0.5, d_b/d_0=0.5, $x_0\,/\,L$=0.004, L=1m.

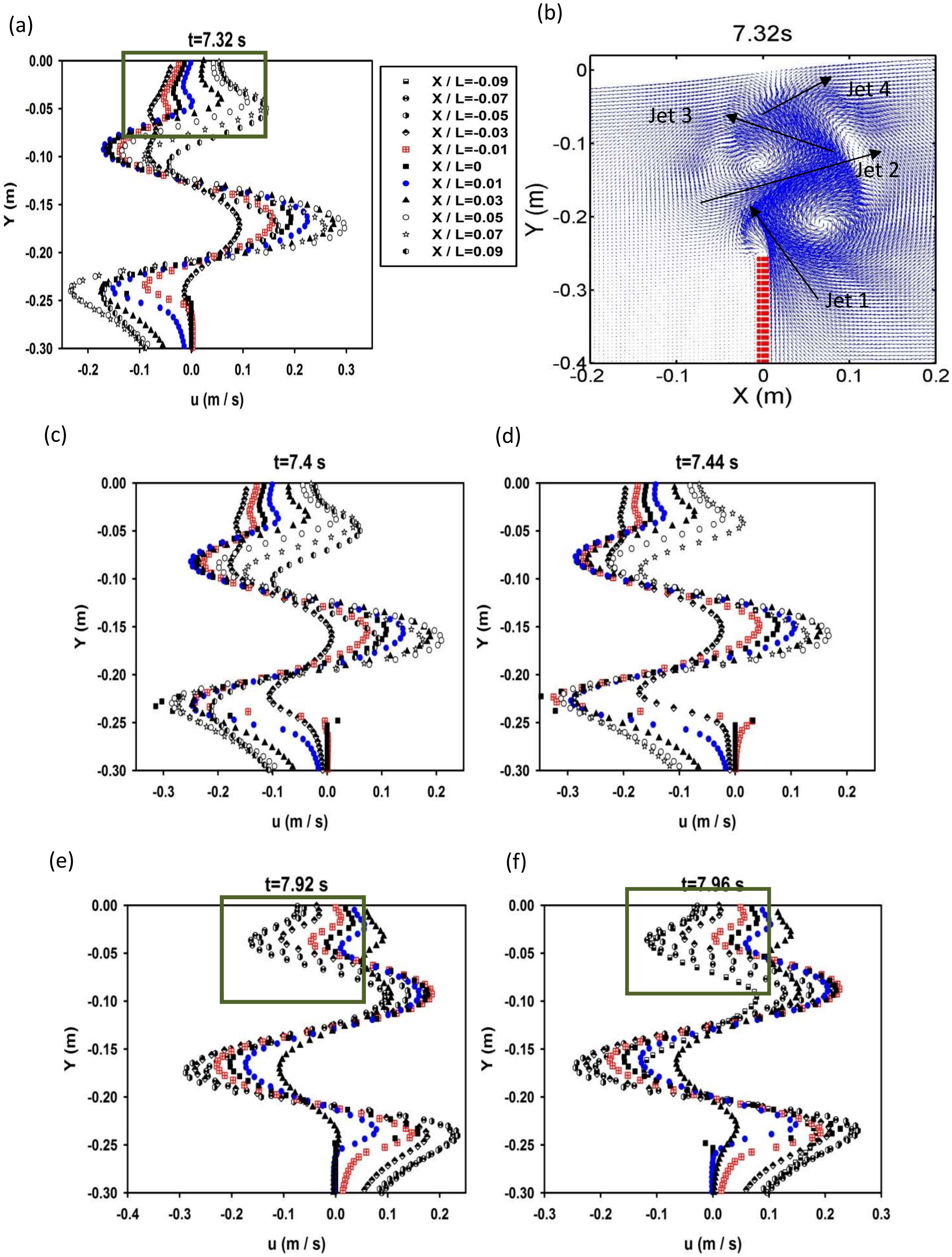

Fig. 18 Variation of the horizontal velocity distribution at eleven vertical cross sections between X / L = -0.1 and 0.1.

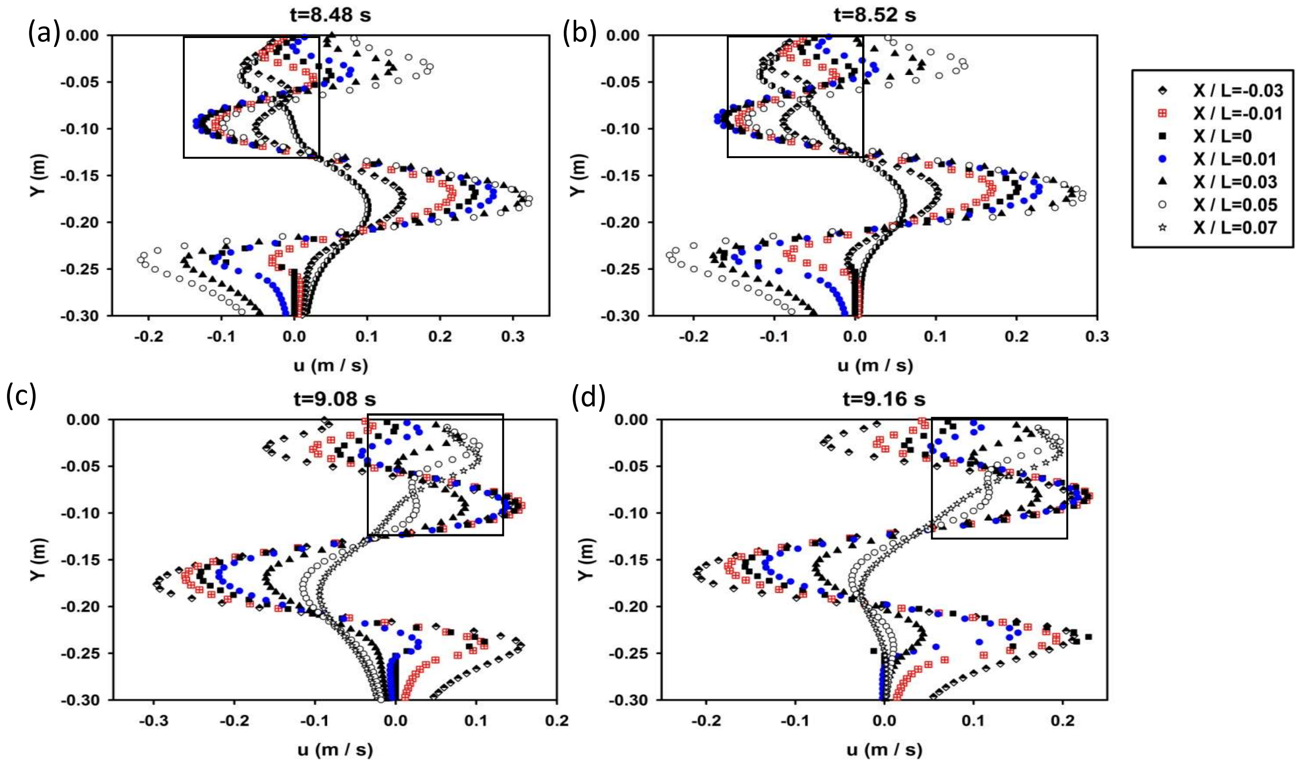

Fig. 19 Variation of the horizontal velocity distribution at seven vertical cross sections between X / L = -0.1 and 0.1.

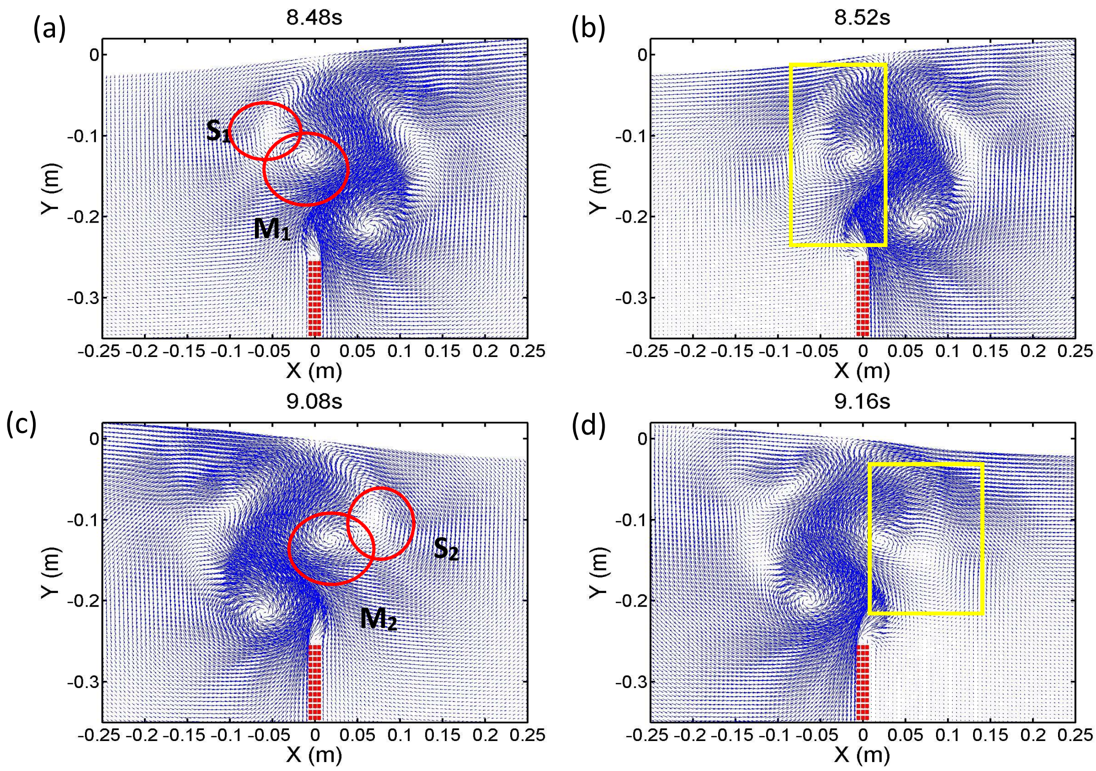

Fig. 20 The velocity vectors of selected times. (a)&(b) the interaction between vortices M_1 and S_1; (c)&(d) the interaction between vortices M_2 and S_2.

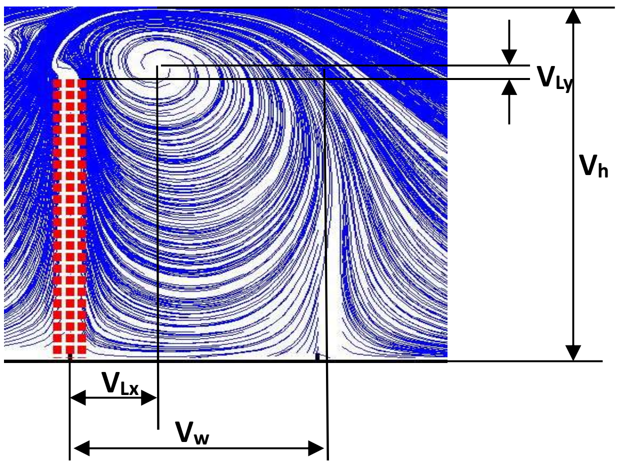

Fig. 21 The streamline of a vortex; location (**V_x,V_y**): the vortex centre; **V_w**: the length of the vortex; **V_h**: the height of the vortex.

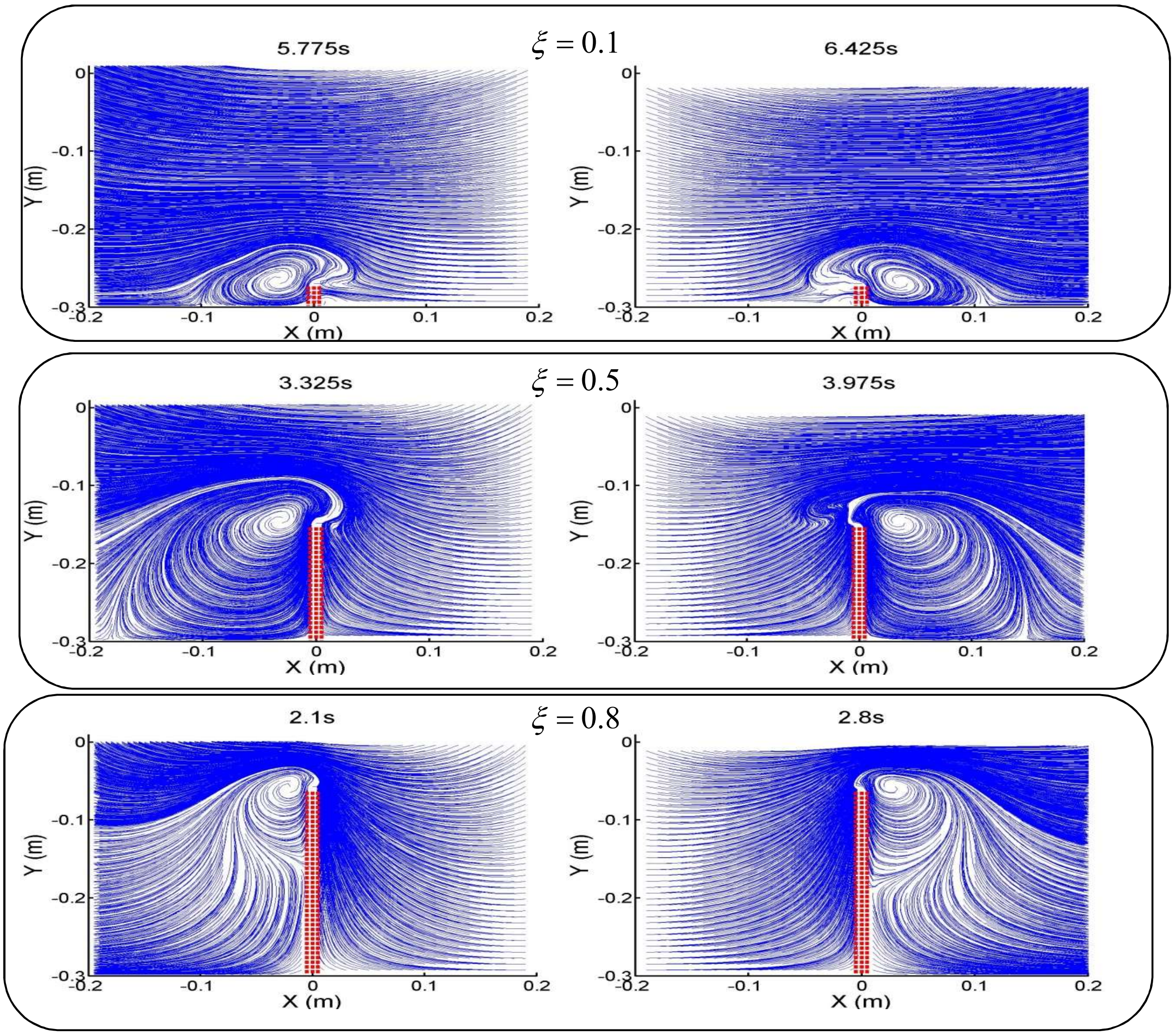

Fig. 22 The streamline of a tank with various ratios of baffle height to liquid depth. d_0/L=0.3, x_0/L=0.002, ω_x=1.05ω_1.

Table 1 The non-dimensional scales of vortices shown in Fig. 22.

ξ	V_{Lx}/d_0	V_{Ly}/d_0	V_w/d_0	V_h/d_0
0.1	0.111	0.013	0.328	0.266
0.2	0.141	0.034	0.382	0.354
0.3	0.118	0.02	0.402	0.444
0.4	0.108	0.017	0.463	0.548
0.5	0.114	0.020	0.507	0.667
0.6	0.101	0.013	0.432	0.744
0.7	0.1	0.017	0.317	0.696
0.8	0.08	0.01	0.226	0.466

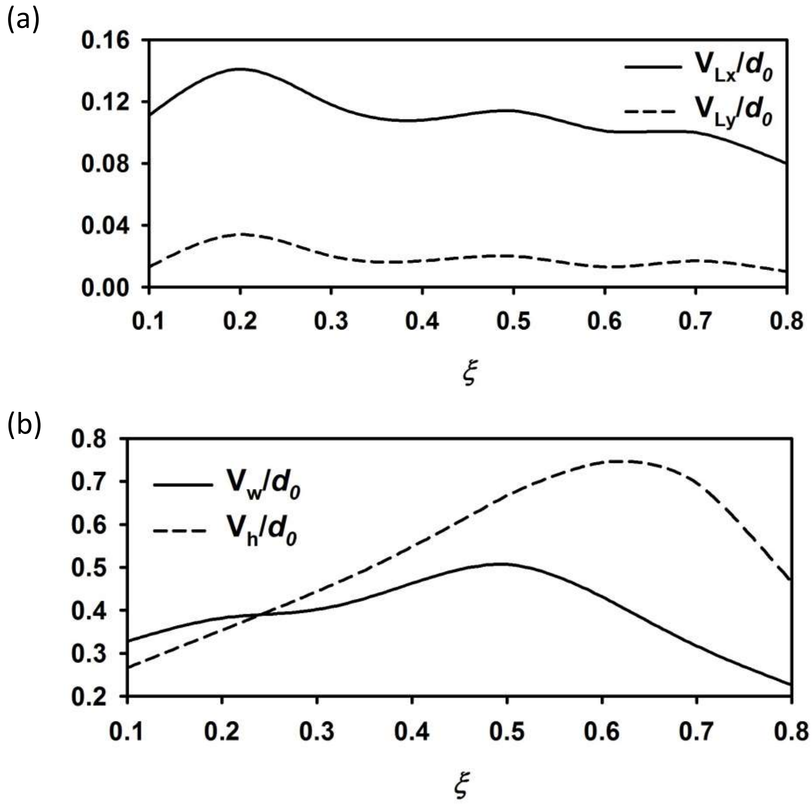

Fig. 23 The size of the vortices under various baffle heights shown in Fig. 22.

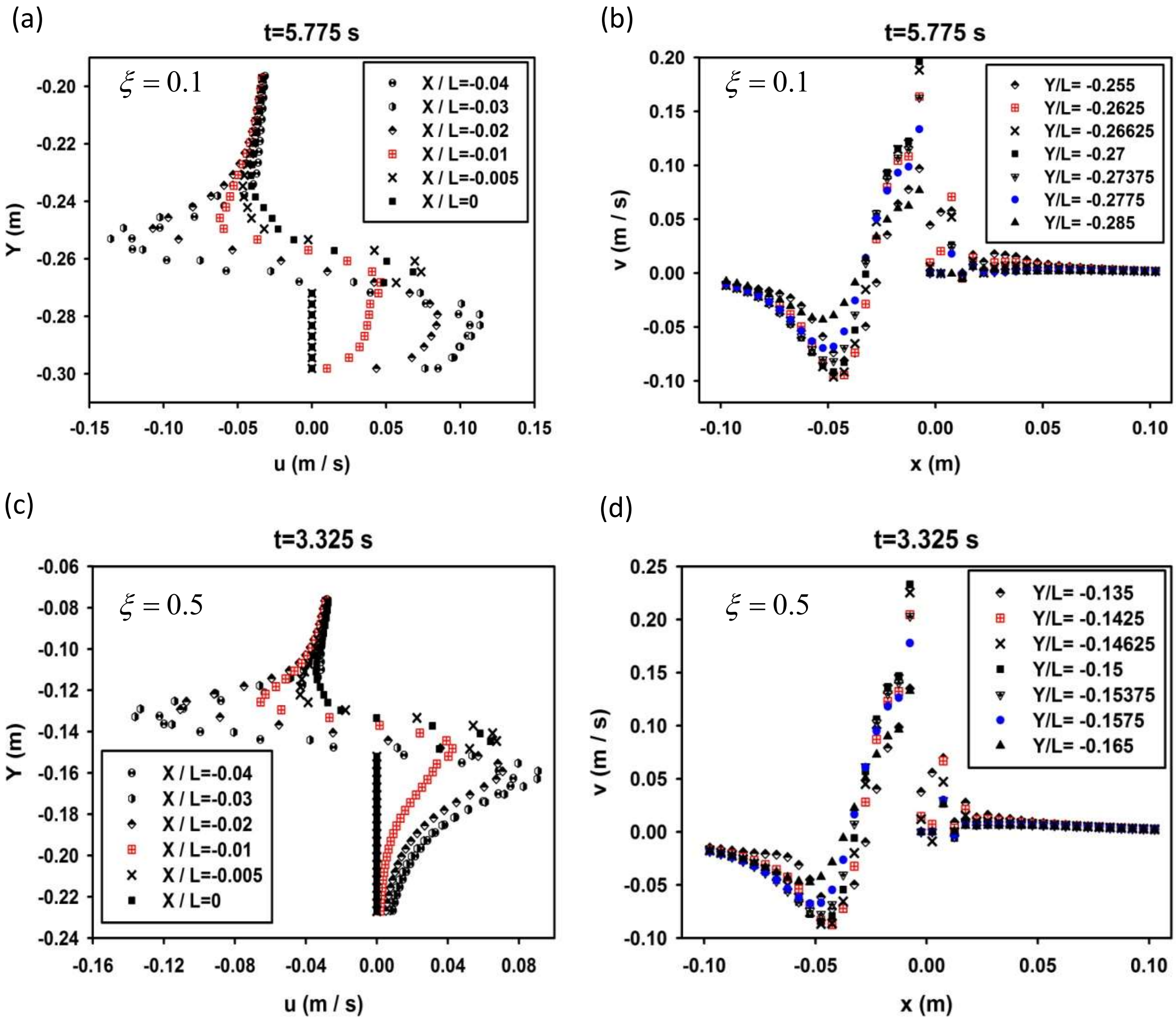

Fig. 24 Variation of the horizontal and vertical velocities distribution correspond to six vertical and seven horizontal cross sections under different d_b / d_0 . d_0 / L=0.3, x_0 / L=0.002, ω_x=1.05ω_1

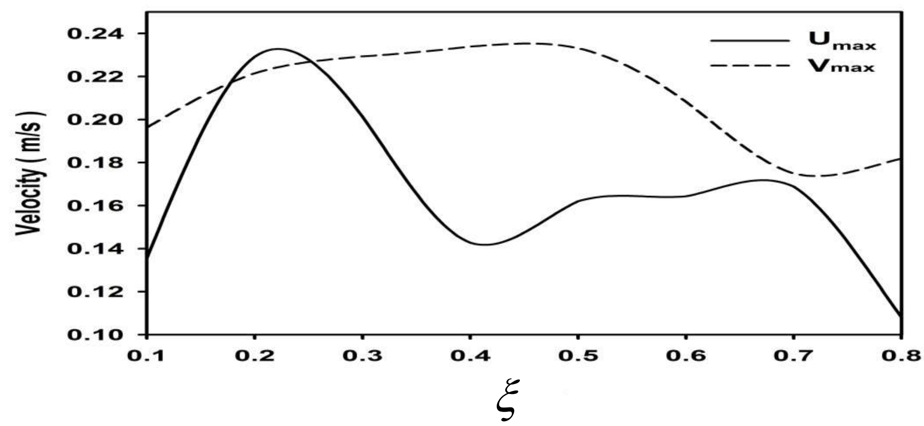

Fig. 25 the maximum horizontal and vertical velocities of the vortices under various baffle heights shown in Fig. 22.

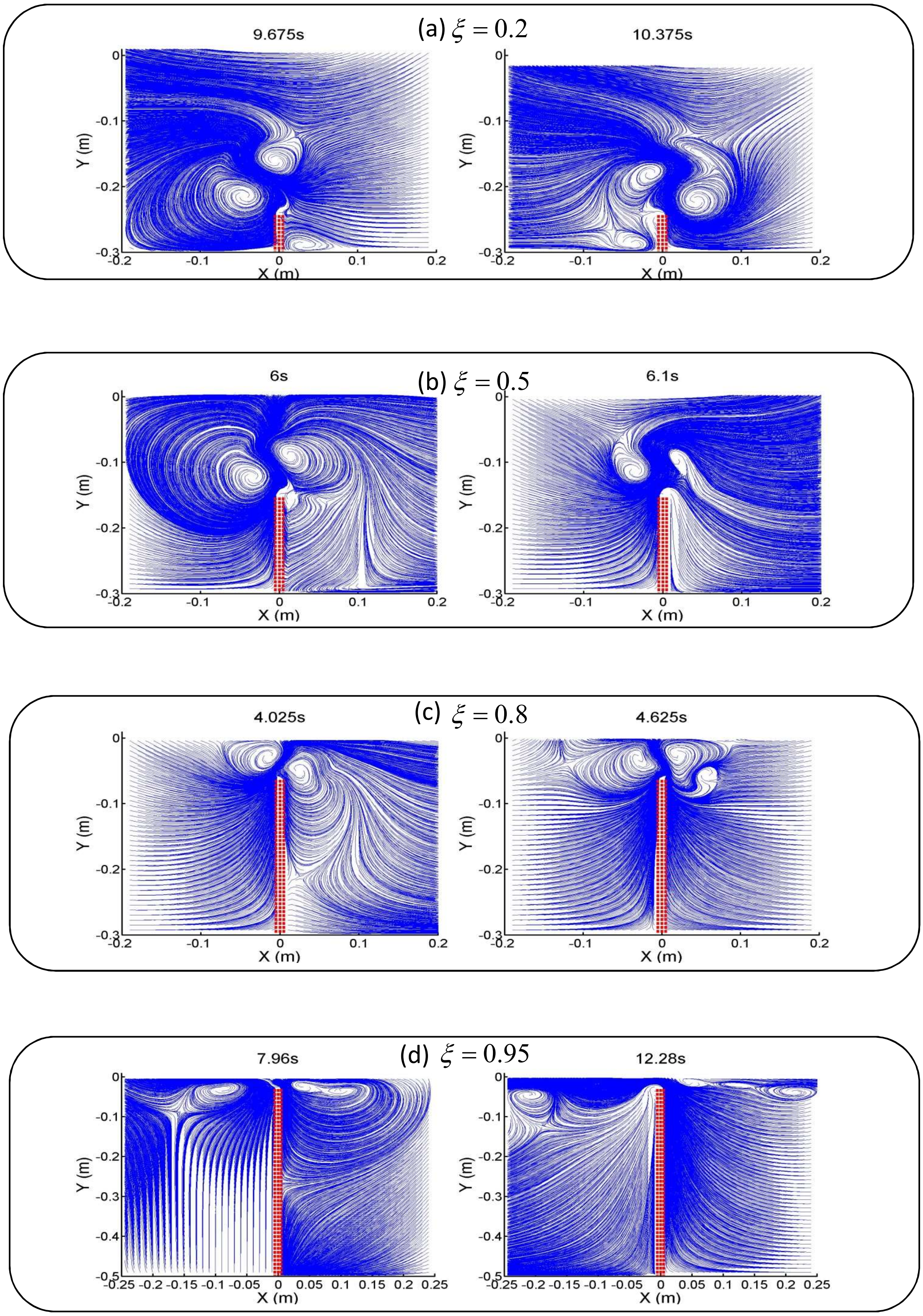

Fig. 26 The streamline of a tank with a vertically bottom-mounted baffle. d_0 / L=0.5, x_0 / L=0.002. The first three cases: ω_x=1.05ω_1, the last case: ω_x=0.6ω_1

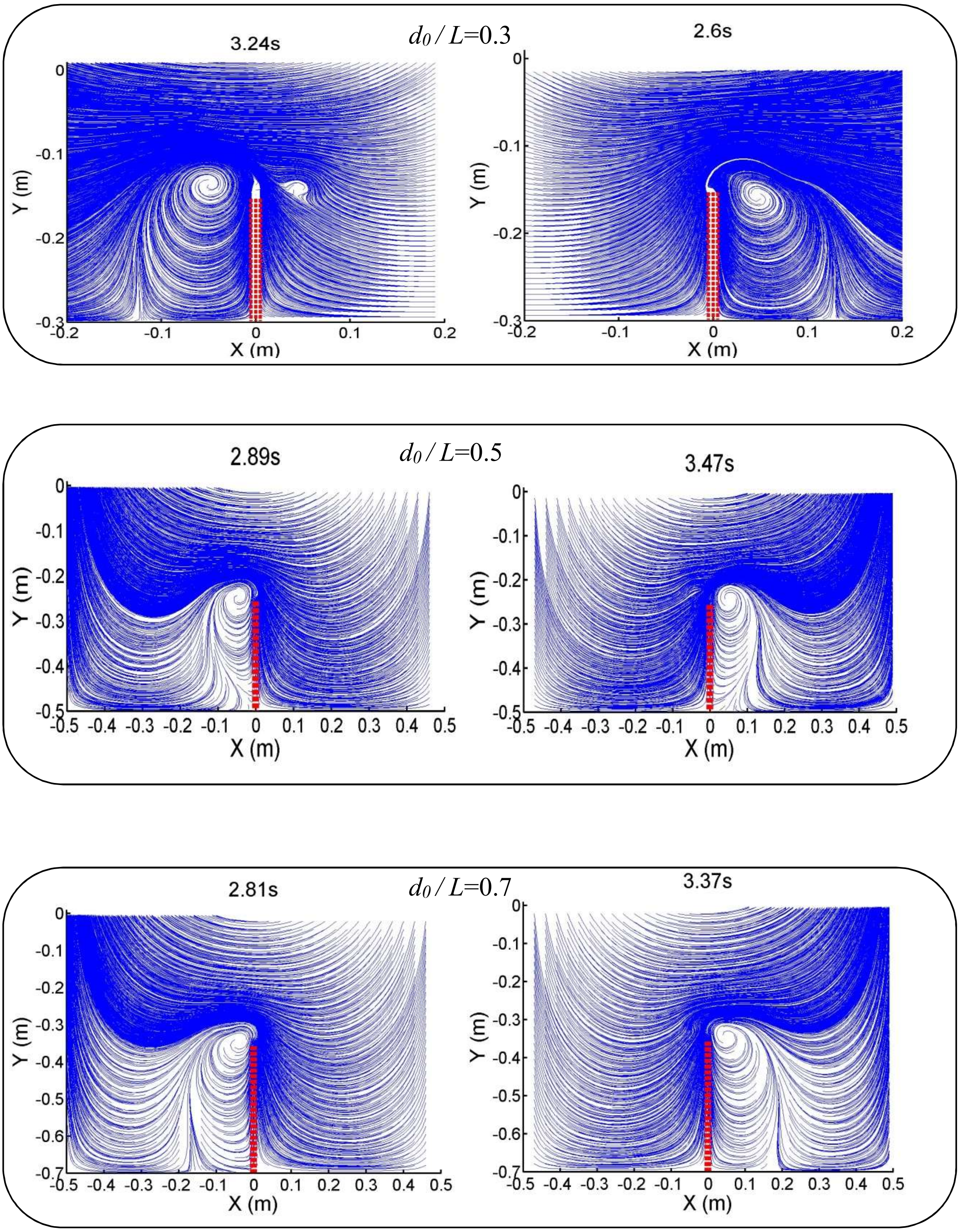

Fig. 27 The streamline of a baffled tank under various water depths. x_0 / L=0.004, ξ =0.5, ω_x=1.05ω_1

Table 2 The non-dimensional scales of vortices shown in Fig. 27.

d_0 / L	V_{Lx}/ L	V_{Ly}/ L	V_w/ L	V_h/ L
0.3	0.048	0.005	0.121	0.187
0.5	0.0465	0.014	0.119	0.267
0.7	0.036	0.014	0.125	0.368

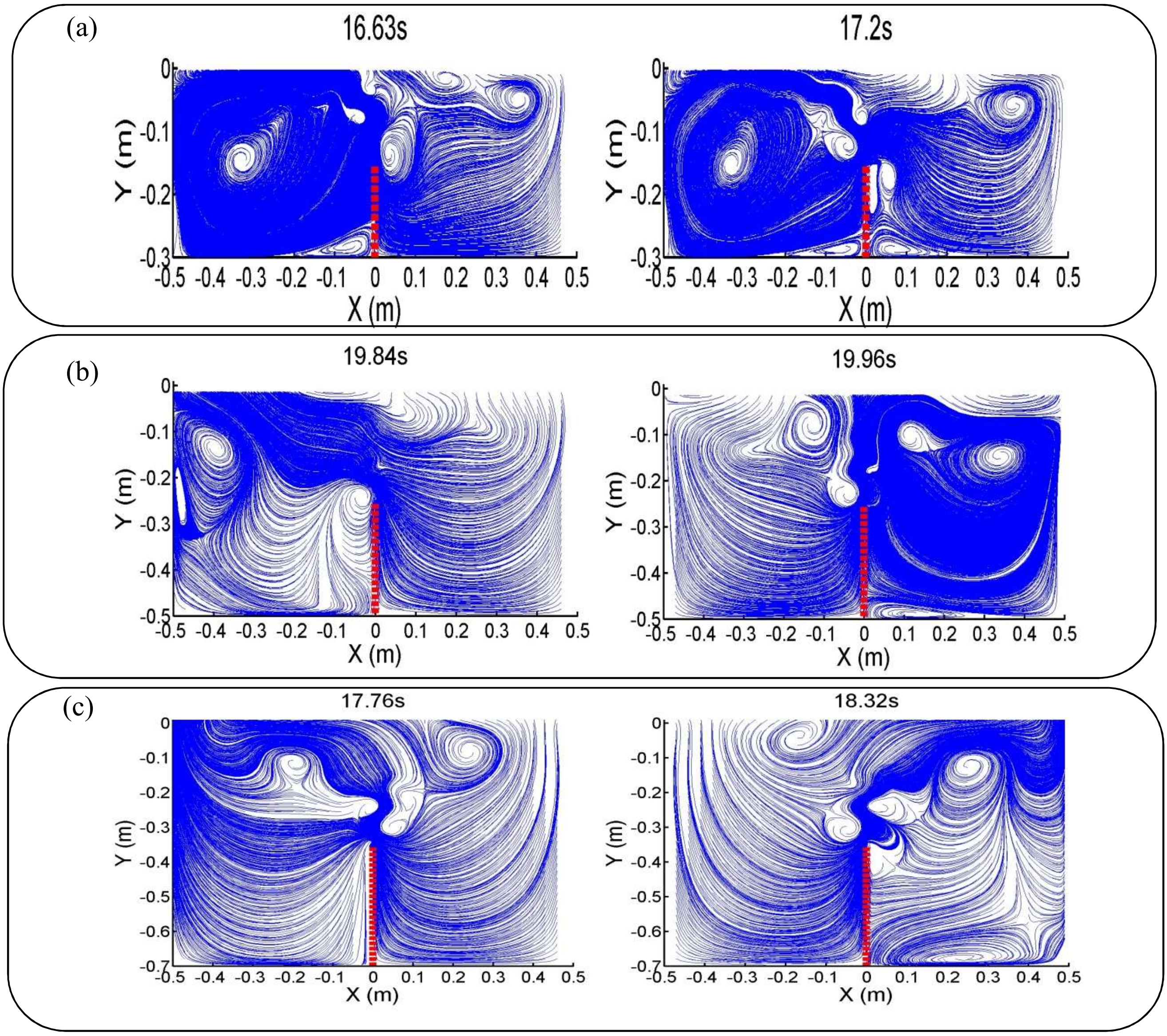

Fig. 28 The streamline of a tank with a vertically bottom-mounted baffle during the transient stage. x_0 / L=0.004, ξ =0.5, ω_x=1.05ω_1 (a) d_0 / L=0.3; (b) d_0 / L=0.5; (c) d_0 / L=0.7.

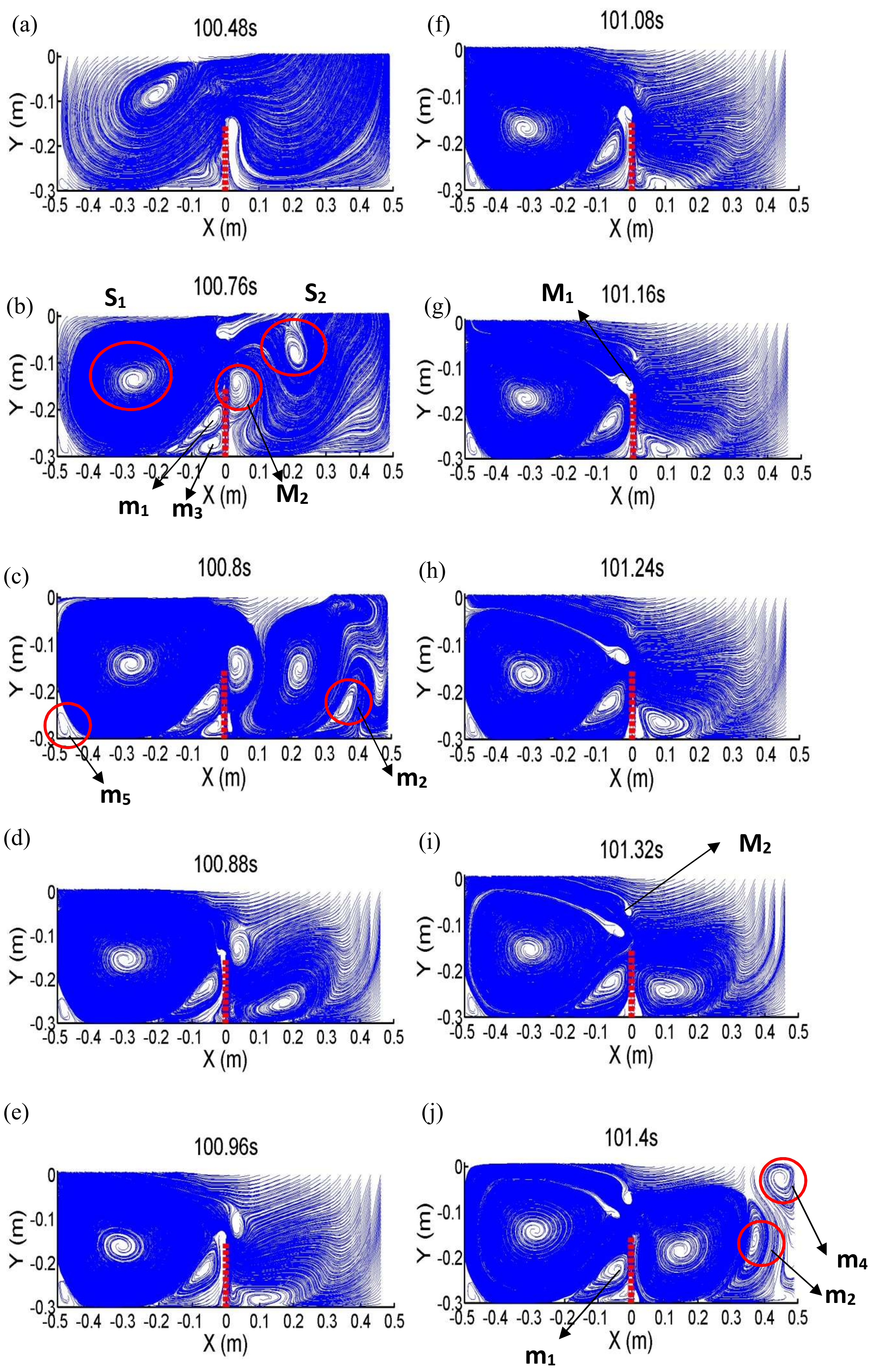

(a)
100.48s
(b)
100.76s
S1
S2
M2
m1
m3
(c)
100.8s
m5
m2
(d)
100.88s
(e)
100.96s
(f)
101.08s
(g)
101.16s
M1
(h)
101.24s
(i)
101.32s
M2
(j)
101.4s
m4
m2
m1
Y (m)
X (m)

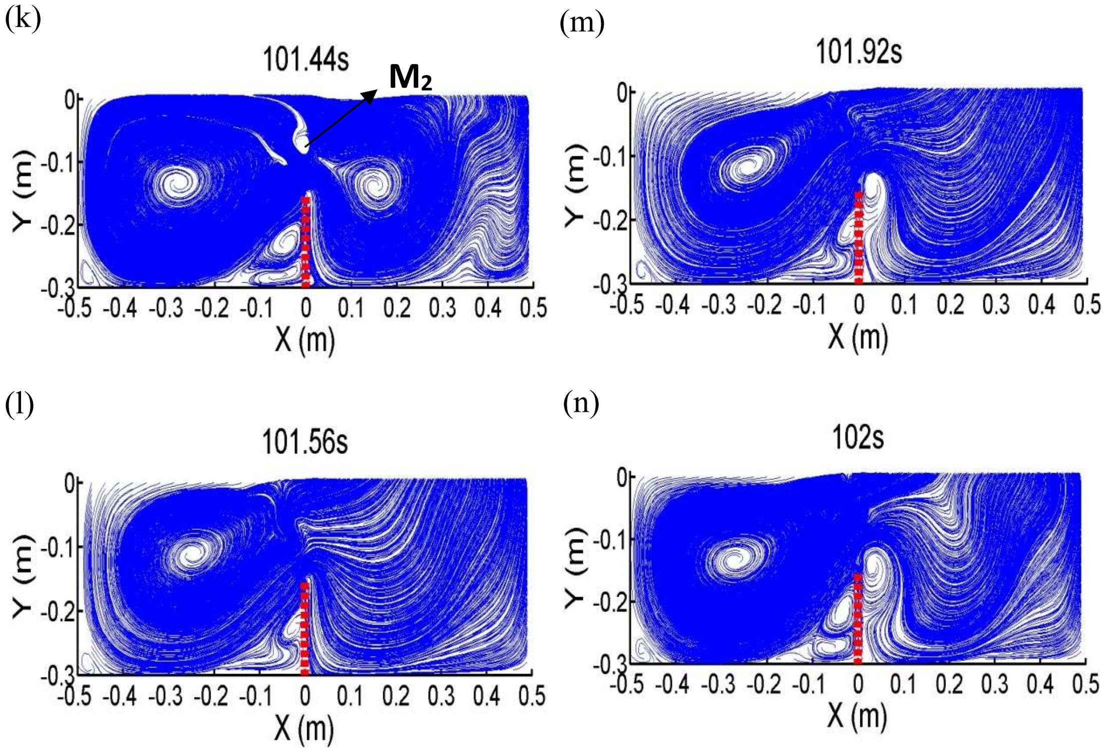

Fig. 29 The streamline of a tank with a vertically bottom-mounted baffle during the steady-state period. d_0 / L=0.3, x_0 / L=0.004, d_b / d_0=0.5, ω_x=1.05ω_1

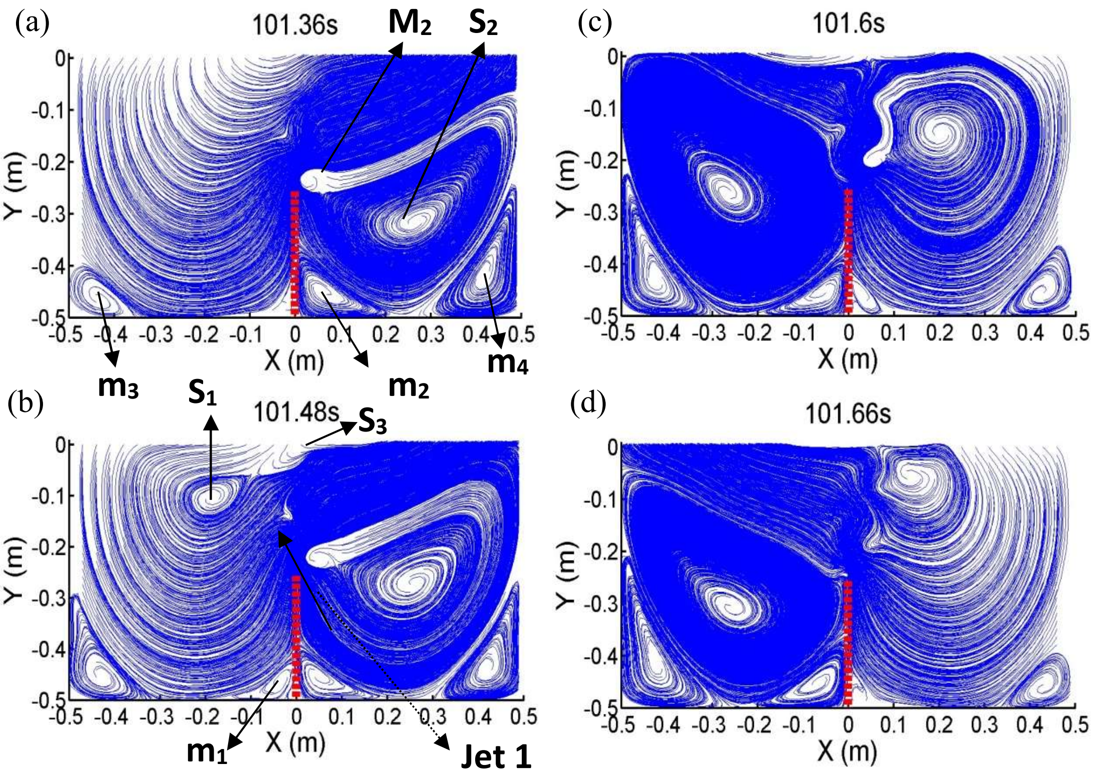

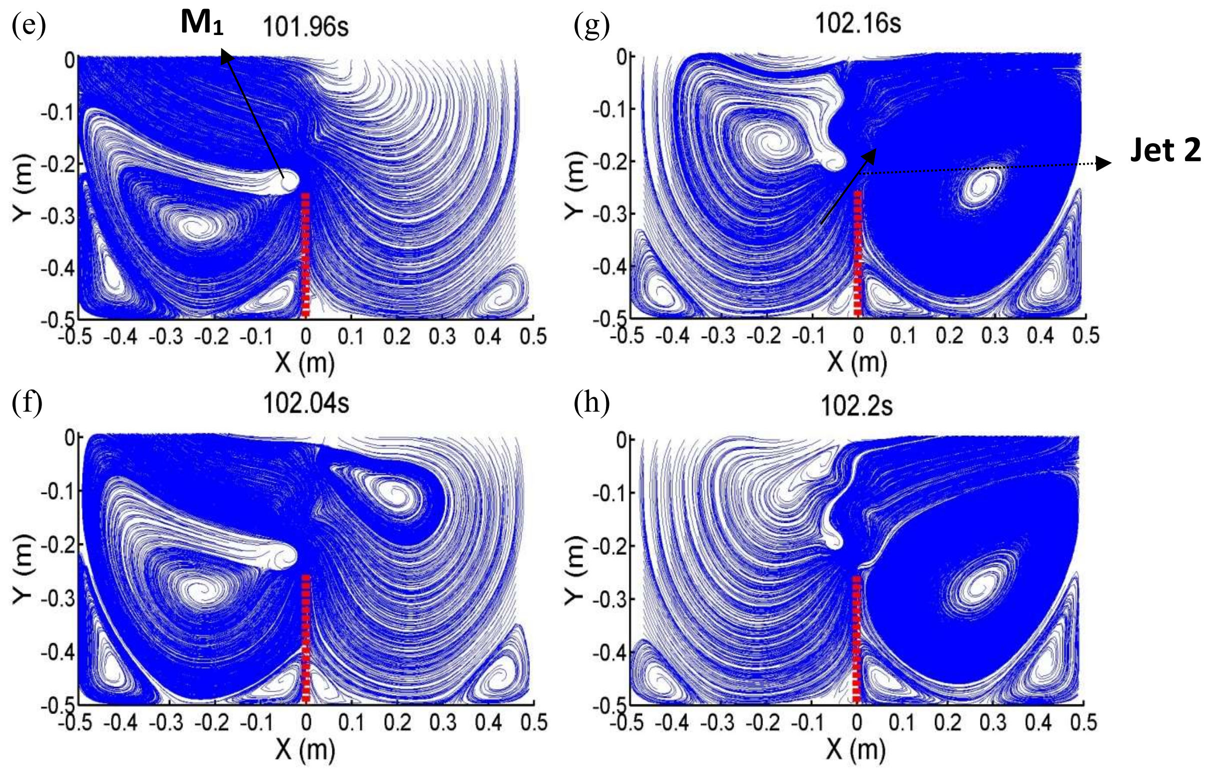

Fig. 30 The streamline of a tank with a vertically bottom-mounted baffle during the steady-state period. d_0/L=0.5, x_0/L=0.004, d_b/d_0=0.5, ω_x=1.05ω_1

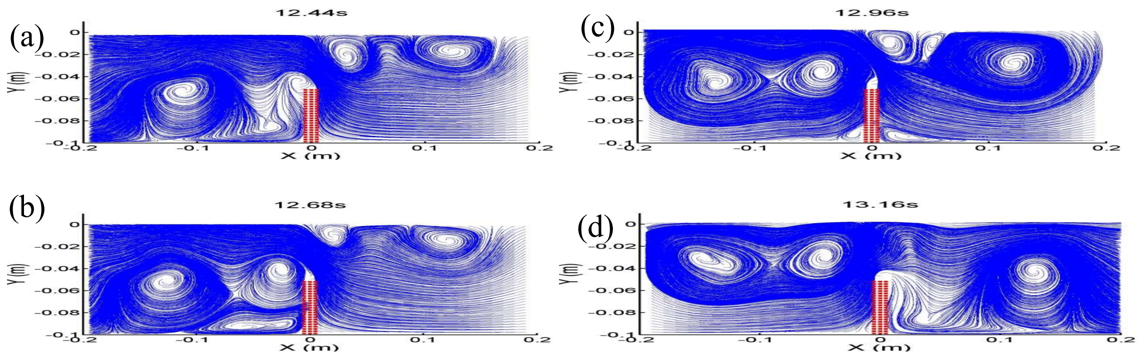

Fig. 31 The streamline of a tank with a vertically bottom-mounted baffle during the transient period. d_0/L=0.1, x_0/L=0.003, d_b/d_0=0.5, $\omega_x = 1.05\omega_1$

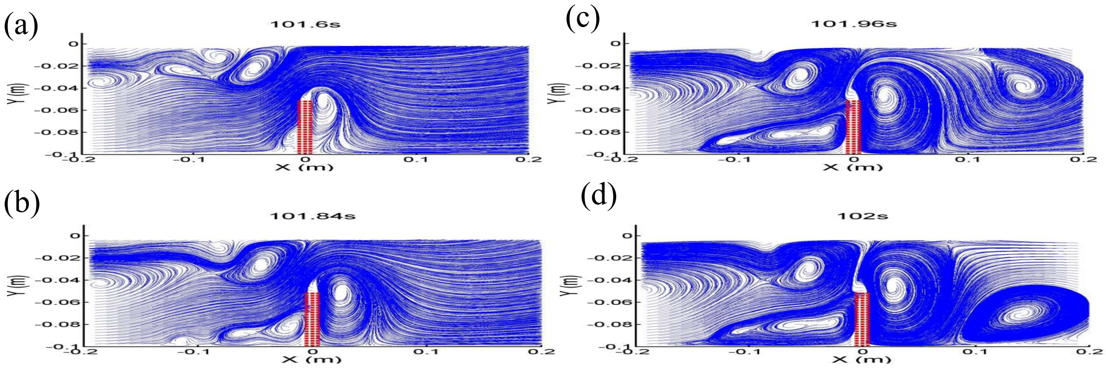

Fig. 32 The streamline of a tank with a vertically bottom-mounted baffle during the steady-state period. d_0/L=0.1, x_0/L=0.003, d_b/d_0=0.5, ω_x=1.05ω_1